eng

MDPI

Article

Quantifying Small-Scale Hyporheic Streamlines and Resident Time under Gravel-Sand Streambed Using a Coupled HEC-RAS and MIN3P Model

Md Abdullah Al Mehedi [1], Munshi Md. Shafwat Yazdan [2,*], Md Tanvir Ahad [3], Wisdom Akatu [1], Raaghul Kumar [2] and Ashiqur Rahman [4]

[1] Department of Civil and Environmental Engineering, Villanova University, Villanova, PA 19085, USA; mmehedi@villanova.edu (M.A.A.M.); wakatu@villanova.edu (W.A.)
[2] Civil and Environmental Engineering, Idaho State University, Pocatello, ID 83209, USA; raaghulkumar@isu.edu
[3] School of Aerospace and Mechanical Engineering, University of Oklahoma, Norman, OK 73019, USA; md.tanvir.ahad-1@ou.edu
[4] Center for Midstream Management and Science, Lamar University, 4400 S M L King Jr Pkwy, Beaumont, TX 77705, USA; ashiqur1912@gmail.com
* Correspondence: yazdmuns@isu.edu; Tel.: +1-208-240-7480

Abstract: Distribution of the water flow path and residence time (HRT) in the hyporheic zone is a pivotal aspect in anatomizing the transport of environmental contaminants and the metabolic rates at the groundwater and surface water interface in fluvial habitats. Due to high variability in material distribution and composition in streambed and subsurface media, a pragmatic model setup in the laboratory is strenuous. Moreover, investigation of an individual streamline cannot be efficiently executed in laboratory experiments. However, an automated generation of water flow paths, i.e., streamlines in the hyporheic zone with a range of different streambed configurations could lead to a greater insight into the behavior of hyporheic water flow. An automated approach to quantifying the water flow in hyporheic zone is developed in this study where the surface water modeling tool, HER-RAS, and subsurface water flow modelling code, MIN3P, are coupled. A 1m long stream with constant water surface elevation of 2 cm to generate hydraulic head gradients and a saturated subsurface computational space with the dimensions of x:y:z = 1:0.1:0.1 m is considered to analyze the hyporheic exchange. Response in the hyporheic streamlines and residence time due to small-scale changes in the gravel-sand streambed were analyzed. The outcomes of the model show that the size, shape, and distribution of the gravel and sand portions have a significant influence on the hyporheic flow path and HRT. A high number and length of the hyporheic flow path are found in case of the highly elevated portion of gravel pieces. With the increase in the base width of gravel pieces, the length of hyporheic flow path and HRT decreases. In the case of increased amounts of gravel and sand portions on the streambed, both the quantity and length of the hyporheic flow path are reduced significantly.

Keywords: groundwater; HEC-RAS; MIN3P; hyporheic exchanges; residence time; model coupling

check for updates

Citation: Mehedi, M.A.A.; Yazdan, M.M.S.; Ahad, M.T.; Akatu, W.; Kumar, R.; Rahman, A. Quantifying Small-Scale Hyporheic Streamlines and Resident Time under Gravel-Sand Streambed Using a Coupled HEC-RAS and MIN3P Model. *Eng* **2022**, *3*, 276–300. https://doi.org/10.3390/eng3020021

Academic Editor: George Z. Papageorgiou

Received: 13 April 2022
Accepted: 7 June 2022
Published: 13 June 2022

Publisher's Note: MDPI stays neutral with regard to jurisdictional claims in published maps and institutional affiliations.

Copyright: © 2022 by the authors. Licensee MDPI, Basel, Switzerland. This article is an open access article distributed under the terms and conditions of the Creative Commons Attribution (CC BY) license (https://creativecommons.org/licenses/by/4.0/).

1. Introduction

The interlinkage between surface water and groundwater is an important phenomenon to perceive the hydrology and water cycle as they can be considered as a single resource and variation in one resource has significant impact over the other [1–3]. This interplay between them plays a critical role in the management and preservation of dependent riparian habitat and ecosystem [4–6]. Groundwater resource comprises more than one-fourth of the total global fresh water [7] and approximately two billion people throughout the world obtain drinking water from this resource [7]. Despite the fact that a very narrow segment of global fresh water is comprised of surface water bodies, e.g., streams, lakes, and rivers apart from

the subsurface water resources, these are easily accessible and also are important water resources for broad usage [8]. Deterioration of water quality and the aquatic ecosystem occur due to the existence of critical solutes resulting in restrictions in water use. The main contributions of these critical substances are collaborated with anthropogenic activities that pave the way to many contaminants to the environment and subsequently to the hydrologic circle [9–11]. Extreme emissions of nitrate and ammonia by intense agricultural activity, sewage water, heavy industrial manufacturing process and the burning of fossil fuels aid the process of eutrophication [12–16]. Surface and subsurface water bodies are hydraulically linked in most of the cases demonstrating a single resource [17–19]. Exchange that happens between surface and groundwater is found to accelerate the contamination of either of the sources by the other [18–20]. The fate and transport of the environmental contaminants and other substances are significantly influenced by the interaction between surface water and groundwater [20–23]. Nonetheless, critical substances at the interface of the surface and groundwater bodies are transformed and retrograded by the various microbial activity. This type of phenomenon is controlled by the dissolved oxygen and carbon sources available [23–25].

Variation between the groundwater and surface water is attributed to the hydraulic gradients, which is the primary reason the water and solutes exchange at the interface [26]. This phenomenon results in downwelling flow, i.e., flow from surface water bodies to the groundwater bodies or upwelling flow, i.e., flow from groundwater bodies to the surface water bodies. The water flow over various streambed morphologies, e.g., pool-riffles, ripples or similar obstacles, water surface profile changes, i.e., hydraulic head gradients, which contribute to the groundwater-surface water exchange or hyporheic exchange [27–32]. This creates a groundwater-surface water exchange zone, where water infiltrates into the subsurface domain, and exfiltrates back to the surface water flow [6]. In recent years, hypothetic exchange within the surface water and groundwater bodies has appeared as an important topic among the researchers to observe the linkage among riverine ecosystem, fluvial geomorphology and groundwater [33,34]. The industrial water waste discharged to the streams can significantly increase nutrient concentrations resulting in a change of hyporheic conditions, e.g., depletion of oxygen concentration. In addition, anthropogenic nutrients, pesticides, and heavy metals can be transported from groundwater into surface water bodies, making the hyporheic zone toxic for living [35–37].

Researchers recognized that there is significant exchange of water, sediments, and nutrients in the surface and groundwater interface. However, the underlying dynamic processes involved are fraught with limited insight and therefore have become problematic [5]. To augment the understanding of hydrologic processes of hyporheic exchange, there is the need for further insight on the mechanisms, by which water, materials, and energy are transferred in the hyporheic zone. Many researchers have resorted to a multifaceted approach towards unraveling the dynamics underpinning surface and groundwater interactions to deal with the challenges associated with these mechanisms. This has also led to the continuous advocacy for active research in combining/coupling physics-based numerical models to estimate hyporheic flow [38–40]. The timing of hyporheic exchange, i.e., the residence time is a determining factor of the ecological and biogeochemical transformation in the hyporheic zone. As water flows through the hyporheic zone, microbial reactions alter its chemical composition with time. The amount of time that a particle spends in a particular system (e.g., subsurface environment) is referred to as residence time. The groundwater component is mostly defined by long residence times, unchanging morphology and laminar flow, whereas the surface water is characterized by turbulence, short residence times, variable discharge, and a dynamic morphology [23,41]. The distribution and quantification of residence times give an indication of the processes involved in holding and releasing water and solutes within the catchment. This controls the concentrations of contaminants and nutrients in the sediment and surface water [36]. Additionally, the catchment residence determines the storage, flow pathways and the source of water and solutes. For instance, evaporation, precipitation, groundwater flow, or stream bed

morphology may have influence on the residence time. Hence, catchment processes can be defined by the distribution of residence times that may also be stated as an indicator of hydrogeochemical and anthropogenic events [34].

Hyporheic residence times and streamline lengths are strongly influenced by riverbeds. An undulant riverbed diverts currents, creating hydraulic gradients along the soil–water interface that works as a driver of hyporheic exchange [27,42–45]. Hyporheic streamlines or flow fields are also highly sensitive to the meanders in stream, which is also dependent on bedform morphology [27,28,44–49]. The automated generation of hyporheic streamlines, with various streambed setups, could help to bring a better understanding of the process and behavior of hyporheic streamlines and residence time distribution under different streambed conditions, whereas this is not the case in laboratory experiments [48]. Moreover, it is not possible for repeatability of results, a high number of variations, greater insight into the three-dimensional system, understanding of individual streamlines or hyporheic residence time distribution to be well executed in the laboratory setup. These circumstances create the need for numerical modeling of the flume experiment to better understand the principal hydro-geo-chemical mechanisms at research and work, which are arduous to isolate under a natural in-stream environment. The hydraulic head differs over a channel bed, is scaled up with the obstacle size, and has a larger impact on comparably shallow surface water compared to deep surface water depth, depending on the obstacle size.

Therefore in line with this assertion, this paper introduced a novel automated framework to compute the hyporheic streamlines and corresponding residence times for a large number of streambed configurations, using a coupled surface water and subsurface water flow modelling tool (HEC-RAS and MIN3P). MATLAB is used to automate the entire process from getting hydraulic head gradient as input due to the variation in streambed configuration to computing streamlines and residence times. To delve into the sensitivity of hyporheic exchange in streambed morphology, the objective of this research is to explore the potential effects of streambed morphology on hyporheic streamlines and residence time distribution, couple surface water and groundwater models to generate a subsurface velocity vector field in an automated process, develop a numerical code to trace particles seeded from the bottom of the streambed, hence, to the top of the subsurface model domain. The paper is divided into four chapters, namely: introduction; data and methods; results and discussions; and conclusion. The project justification, objectives, and delineation of the theories behind GW–SW interactions and hyporheic exchange are presented in the introduction chapter. In data and methods, strategies, and techniques to quantify hyporheic exchange in terms of streamline distributions and residence time are discussed. The outcomes and detailed discussions of the research are illustrated in the results and discussions chapter. The conclusion chapter summarizes the research outcome and provides recommendations for further studies.

2. Materials and Methods

2.1. Formulation of GW-SW Exchange

A one-dimensional steady flow model is analyzed using a surface water modelling tool, HEC-RAS, to generate the distribution of hydraulic head over the streambed. In this study, the flow regime is set to be subcritical. Figure 1 represents a visualization of the water surface profile with gradient. The Energy equation used to compute the water surface profile is written as follows

$$Z_2 + Y_2 + \frac{a_2 V_2^2}{2g} = Z_1 + Y_1 + \frac{a_1 V_1^2}{2g} + h_e \quad (1)$$

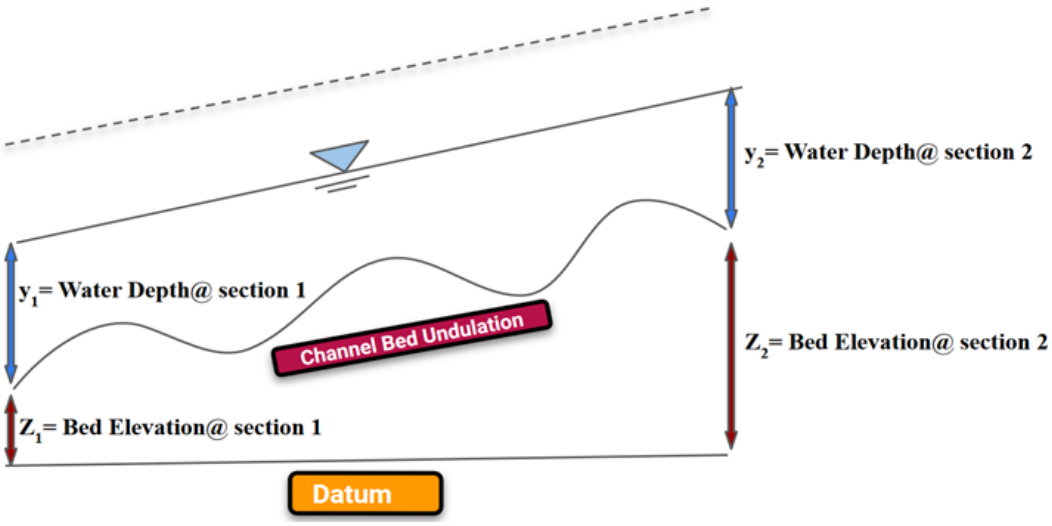


Figure 1. A visualization of the water surface profile with a gradient due to the undulation in streambed for a typical one-dimensional surface water model. Due to the change in elevation of the channel bed, a hydraulic gradient occurs, which is the key parameter to generate hyporheic exchange.

In the above equation, Z_2, Z_1 = bed elevation of the channel bed, Y_2, Y_1 = Water depth; V_1, V_2 = Average velocity; a_1, a_2 = weighting coefficient; g = gravitational acceleration and h_e = head loss.

The energy head loss between two consecutive cross sections consists of friction losses and contraction or expansion losses. The equation for the energy head loss can be written as follows [49]:

$$h_e = LS_f + C\left|\frac{a_2 V_2^2}{2g} - \frac{a_1 V_1^2}{2g}\right| \quad (2)$$

In the above equation, $\boldsymbol{L}$ = discharge weighted reach length.

$\boldsymbol{S_f}$ = friction slope between two sections.

$\boldsymbol{C}$ = contraction or expansion loss coefficient.

Groundwater refers to subsurface water, where the subsurface medium is fully saturated. In this study, a fully saturated subsurface, i.e., groundwater domain is considered. The basic equations for saturated subsurface water flow can be written as [50]

$$\boldsymbol{S}\frac{\partial \boldsymbol{h}}{\partial \boldsymbol{t}} - \nabla.\boldsymbol{q} = \boldsymbol{Q} \quad (3)$$

$$\boldsymbol{q} = -\boldsymbol{K}.\nabla \boldsymbol{h} \quad (4)$$

The above equation is solved for the hydraulic head h and the Darcy flux q, where S is the coefficient of specific storage, $\boldsymbol{K}$ is the hydraulic conductivity and Q denotes source/sink function. By substituting $\boldsymbol{q}$ the Darcy equation can be written in the Richards-type form:

$$S\frac{\partial h}{\partial t} - \nabla.(\boldsymbol{K}.\nabla h) = Q_h + Q_{hw} \quad (5)$$

In the equation above, the source/sink term $Q = Q_h + Q_{hw}$ is a split into a supply term Q_h and a well-related term is Q_{hw}.

In this study, a fully saturated porous media is considered for analyzing particle tracks if seeded from the surface of the model domain. Particles go along the path, which is determined by the velocity vector field present in the model domain.

In the Figure 2, water flow through an element of the streambed can be seen. In this figure, A denotes the cross-sectional area, $\boldsymbol{L}$ denotes length, Q_i and Q_o denote the subsurface inflow and outflow, and e denotes the upwelling or downwelling hyporheic water flux per unit length (L) of streambed [45].

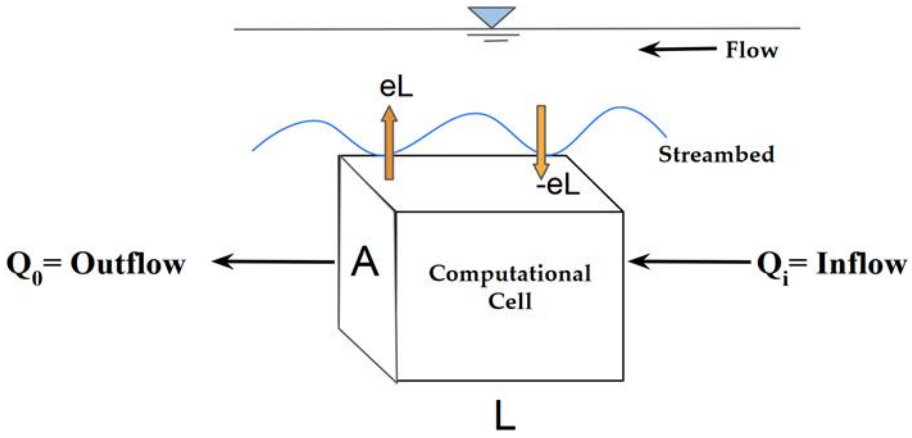


Figure 2. An elementary model to delineate the principal process of hyporheic exchange.

According to the Figure 2, a soil volume in the streambed with a cross-sectional area A and a dimension L was considered. It is assumed that the direction of subsurface flow through the volume is parallel to the sides of the soil element in such a way that no lateral flow happens. Moreover, the bottom of the elementary volume is assumed to be impermeable, and the upper surface contributes the soil–water interface. Therefore, the variation in the total amount of water flow in this volume over time (dV_w/dt) can be written as [51]

$$\frac{dV_w}{dt} = Q_i - Q_o + e.L \tag{6}$$

In case of steady-state conditions where no temporal variation is considered, V_w does not vary with time making $dV_w/dt = 0$, the equation will be written as the following form-

$$e = \frac{Q_o - Q_i}{L} = \frac{\Delta Q}{\Delta l} = \frac{dQ}{dl} \tag{7}$$

The subsurface discharge (Q) can be defined from the equation

$$Q = uA = K\frac{\mathrm{dh}}{dl}A \tag{8}$$

where, K is the soil hydraulic conductivity, u depicts the subsurface flow velocity and dh/dl is the spatial gradient of the hydraulic head. By substituting the discharge term from Equation (8) into the Equation (7) the following equation can be derived.

$$e = \frac{d\left(-KA\frac{dh}{dl}\right)}{dl} = -KA\frac{d^2\mathrm{h}}{dl^2} - K\frac{\mathrm{dA}}{dl}\frac{\mathrm{dh}}{dl} - A\frac{\mathrm{dK}}{dl}\frac{\mathrm{dh}}{dl} \tag{9}$$

In Figure 3, 2D spatial dynamics of hyporheic streamlines due to the undulation in the streambed are illustrated. Variations in extent of the hyporheic streamlines are function of stream bed undulation. In this study, the response in the extent of the hyporheic exchange is explored with a set of streambed configurations and material (e.g., gravel, sand).

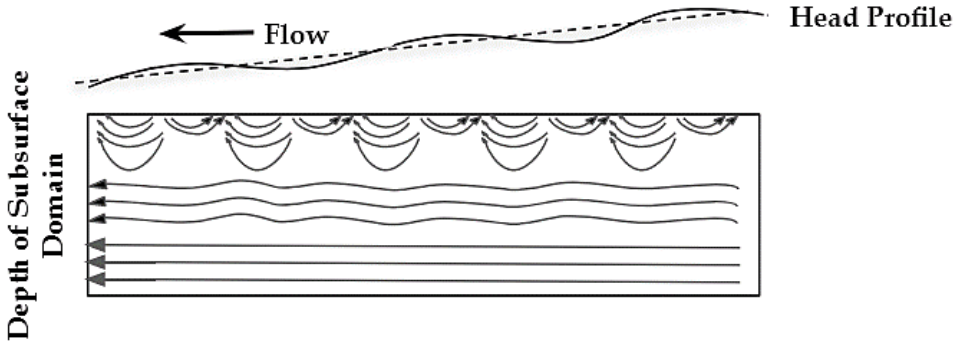


Figure 3. Depth and spatial pattern of hyporheic streamlines described as a function of the Hydraulic head gradient profile.

2.2. Numerical Modelling of Hyporheic Exchange

The surface water model is set up and simulated in the HEC-RAS, which is an executable code developed by U.S. Army Corps of Engineers. Using the streambed geometry mentioned before and initial/boundary as follows, 1D steady surface water models are analyzed. A constant discharge, Q = 0.00006 m^3/s, was considered as a boundary condition for steady flow analysis [50]. The initial condition was a fixed water surface elevation of 0.02 m in the stream. The geometry of the channel is 1m long (x-direction) 0.1 m wide (y direction), 0.1 m high in z-direction. No slope along longitudinal direction of the stream. The minimum distance between cross sections that HEC-RAS can handle without creating instabilities is 0.00025 m. For a reach size of 1 m, the resolution which is found to be too small for HEC-RAS to handle is 0.0001, which would correspond to 10,000,000 cross-sections. Therefore, 1000 cross-sections are considered over the entire stream length to reduce the instability and computational effort. Hydraulic heads are recorded at each cross-section and further used as a top boundary condition of the groundwater model.

MIN3P (multicomponent reactive transport code) is used to prepare the flow field in the subsurface saturated porous media. Spatial discretization is conducted based on the finite volume method, which allows three-dimensional analysis [52,53]. The finite volume method (FVM) is a robust method extensively used in computational fluid dynamics [54]. The global mass conservation for the components is discretized in three-dimensional space, using the FVM in MIN3P by considering fully implicit time weighting [55].

The fourth order Runge–Kutta method is used in this study to trace hyporheic streamlines (Figure 4). The vectors considered in the subsurface water flow field can be written as follows

$$P_{i+1} = P_i + (1/6)\,\Delta t\vec{v}_i + (1/3)\,\Delta t\vec{v}^{\mathbf{1}}_{\boldsymbol{i+1}} + (1/3)\,\Delta t\vec{v}^{\mathbf{2}}_{\boldsymbol{i+1}} + (1/6)\,\Delta t\vec{v}^{\mathbf{3}}_{\boldsymbol{i+1}} \quad (10)$$

where, P_i denotes the beginning position of the streamline, Δt is the time step, $\vec{v}^{1}_{i+1}$ is the flow vector corresponding to the point $P_i + (\frac{1}{2})\Delta t\ \vec{v}_i$, $\vec{v}^{2}_{i+1}$ is the flow vector corresponding to the point $P_i + (\frac{1}{2})\Delta t\ \vec{v}^{1}_{i+1}$ and $\vec{v}^{3}_{i+1}$ is the vector corresponding to the point $P_i + \Delta t\ \vec{v}^{2}_{i+1}$.

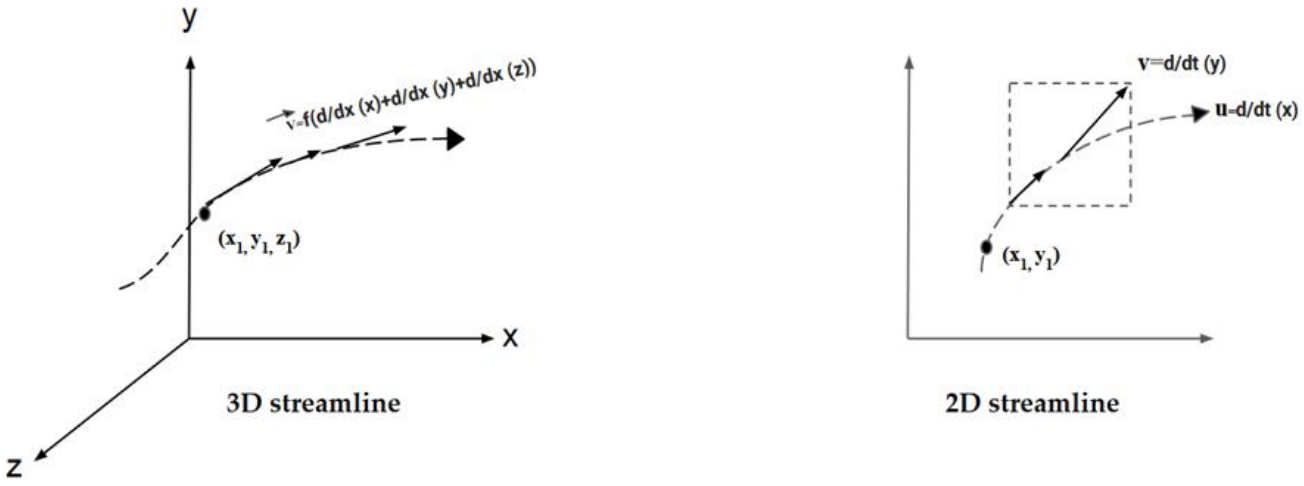


Figure 4. Streamline calculation in both 2-D and 3-D cases.

2.3. Model Parameterization

The streambed used and investigated in the numerical model is prompted by a small scale (e.g., a surface water model domain having a length of 1 m is used in this study) hyporheic exchange with a gravel-sand streambed. An alternating gravel-sand streambed is set up to generate hydraulic head gradient. Impact of the shape and size of gravel pieces and the distribution of gravel and sand portion in the channel bed on hyporheic streamlines and HRT are analyzed. The shapes considered for gravel pieces are trapezoid, rectangle, triangle and circular. In addition to gravel pieces, the impact of gravel bars (trapezoidal) that have a greater dimension along the longitudinal direction of the streambed are investigated. A channel with a 1 m longitudinal length is considered for all the model setups. A constant channel width of 0.1 m is considered for all model setups. Moreover, water surface elevation of 2 cm is used as a known boundary condition for both the upstream and downstream direction. Channel beds are divided into 1000 sections, where every section has a dimension of 1 mm. The elevation of the cross-section at every mm is varied to represent streambed geometry. According to particle size, channel bed elevation is adopted. Gravel, as defined by [55] can have a range of 2mm up to 64mm, so anything within that range is generally considered to be gravel [55,56]. Considering the measured grain size distribution in the experiment conducted by [49], a grain size distribution of 2–10 mm for gravel with an average grain size of d50 = 4.75mm and for sand 0.2–2 mm with an average grain size of d50 = 0.57.The size of gravel pieces is chosen in such a way that it covers the whole range of gravel size [54]. With varying sizes of gravel pieces, hydraulic head distribution varies, and hence, this generates gradient. Proper hydraulic head gradient is considered to be the most important factor for hyporheic exchange. It is the driving force for generating different scaled hyporheic exchange. Manning's roughness coefficient for gravel and sand are selected as per [57–59].

2.3.1. Base Case

Trapezoidal gravel pieces with dimensions of 10 mm as height (h) and base width (b_w) are chosen for base case scenario. The reason for choosing this dimension is the entire length of the channel can be evenly distributed. Moreover, computational nodes of the channel bed for measuring elevation can be evenly distributed. ID of the model setup of the base case is gpt10 × 10. Figure 5a demonstrates a sketch of a single trapezoidal gravel piece and Figure 5b represents a sketch of consecutive gravel pieces.

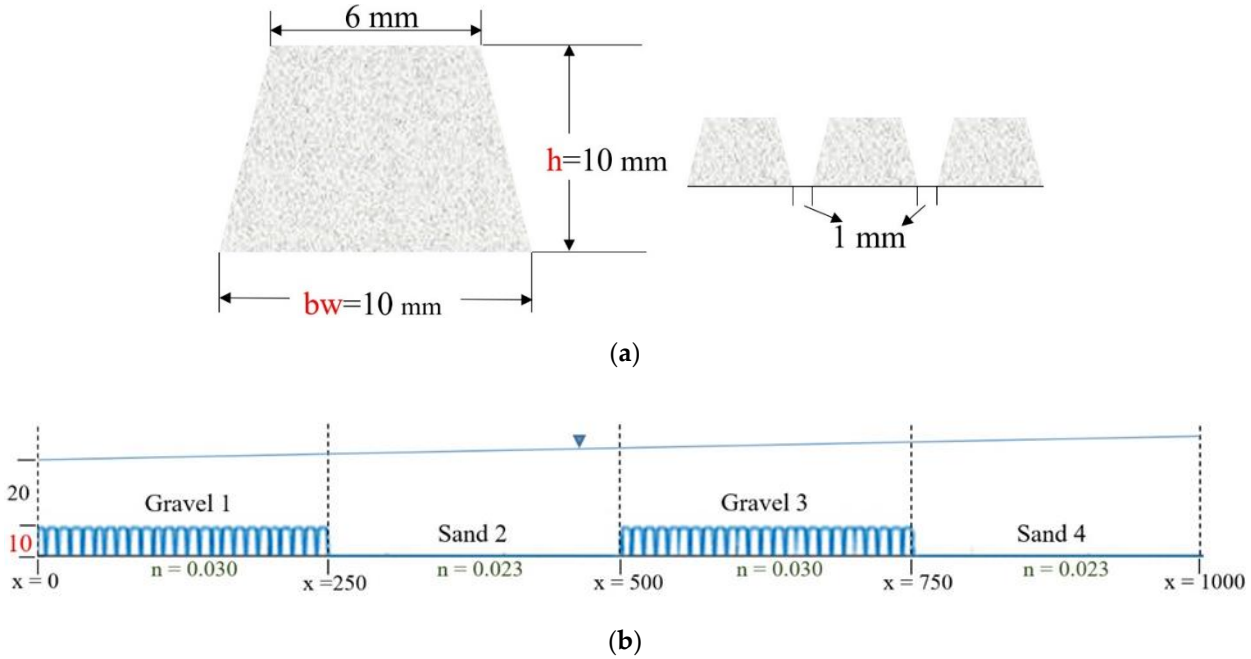


Figure 5. (**a**) Sketch of a single trapezoidal gravel piece with the dimension of 10 mm × 10 mm used as base case. (**b**) Sketch of consecutive gravel pieces with the dimension of a gap among them. Streambed with 10 × 10 trapezoidal gravel pieces is used as a base case. Four zones of gravel and sand with Manning's roughness coefficient, n, can be seen.

2.3.2. Size of the Gravel Piece: Height

The ridges created by the elevated portion of gravel pieces are considered to be the height. This parameter is of paramount importance as it is responsible for generating HH variation over the streambed, and hence, it influences the hyporheic exchange. In Figure 6, the height can be seen, which is denoted by h. In total, six model setups were considered for investigating the impact of height variation over hyporheic streamlines distribution and residence time. In these model setups, only the height was increased from a minimum 2 mm to a maximum of 30 mm. The heights of gravel pieces were selected in such a way that it reduced the complicacy in generating and distributing the nodes necessary to measure and store elevation data of the streambed. Trapezoidal gravel pieces were chosen for the analysis. In Table 1, a summary of model setups can be seen.

Table 1. Model setups for the analysis of the effect of height variation over hyporheic exchange. (h, b_w and l denote the height, base width, and width of top surface of gravel pieces, respectively). Units are mm.

Group	Simulation ID/Model Setup	Description
Height of gravel piece (h)	gpt2 × 10	Trapezoidal gravel particle with h = 2, b_w = 10, l= 6
	gpt5 × 10	Trapezoidal gravel particle with h = 5, b_w = 10, l = 6
	gpt8 × 10	Trapezoidal gravel particle with h = 8, b_w = 10, l = 6
	gpt10 × 10	Trapezoidal gravel particle with h = 10, b_w = 10, l = 6
	gpt20 × 10	Trapezoidal gravel particle with h = 20, b_w = 10, l = 6
	gpt30 × 10	Trapezoidal gravel particle with h = 30, b_w = 10, l = 6

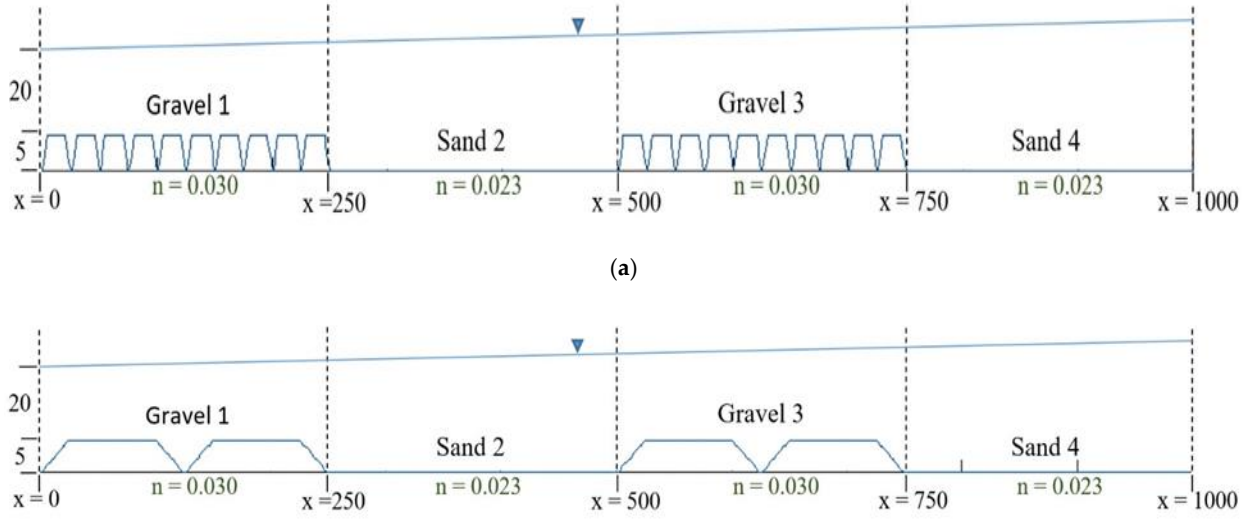


Figure 6. Base width (b_w) of the gravel pieces of the streambed is varied to investigate the effect of base width variation over hyporheic exchange. ID of the model setups are gpt5 × 10 (**a**), and gpt5 × 125 (**b**). All units are in mm.

2.3.3. Base Width

As with height, base width of gravel pieces also plays a vital role in creating variation in water surface elevation above the streambed, thus altering HH distribution. The number of nodes per gravel piece is determined by multiplying the base width of gravel piece by 1000. For example, if the base width is 0.025 m, then the number of nodes will be 0.025 times 1000 and, i.e., 25. After determining the number of nodes per gravel piece, nodes are distributed over a sloping surface and flat surface of the gravel piece. Nodes are set up at every millimeter. The following equations are used to distribute the number of nodes over inclined as well as flat surfaces of the trapezoidal gravel piece.

$$\text{nodes_gr} = \text{b_gr} \times 1000$$

$$\text{nodes_rf} = (\text{nodes_gr}/5)*2;\ \text{nodes_fl} = \text{nodes_gr-nodes_rf}$$

Here, nodes_gr = number of nodes per gravel piece, nodes_rf = Number of nodes on inclined (rising + falling) surfaces, nodes_fl = number of nodes on flat surface of the trapezoidal gravel piece. Figure 6 shows the base width (bw) of the gravel pieces of the streambed is varied to investigate the effect of base width variation over hyporheic exchange (a) gpt5 × 10, and (b) gpt5 × 125.

2.3.4. Variation in the Distribution of Gravel and Sand Portion

Gravel and sand portions are found to be randomly distributed with a variation in the extent of the portions. These differences in the extent and distribution of particles play a crucial role in creating hyporheic exchange. Due to computational limitations, a systematic approach is taken into hand to address the variation in the distribution of gravel and sand portion. In this study, streambeds with varying distribution of gravel and sand portion are set as the following (Figure 7).

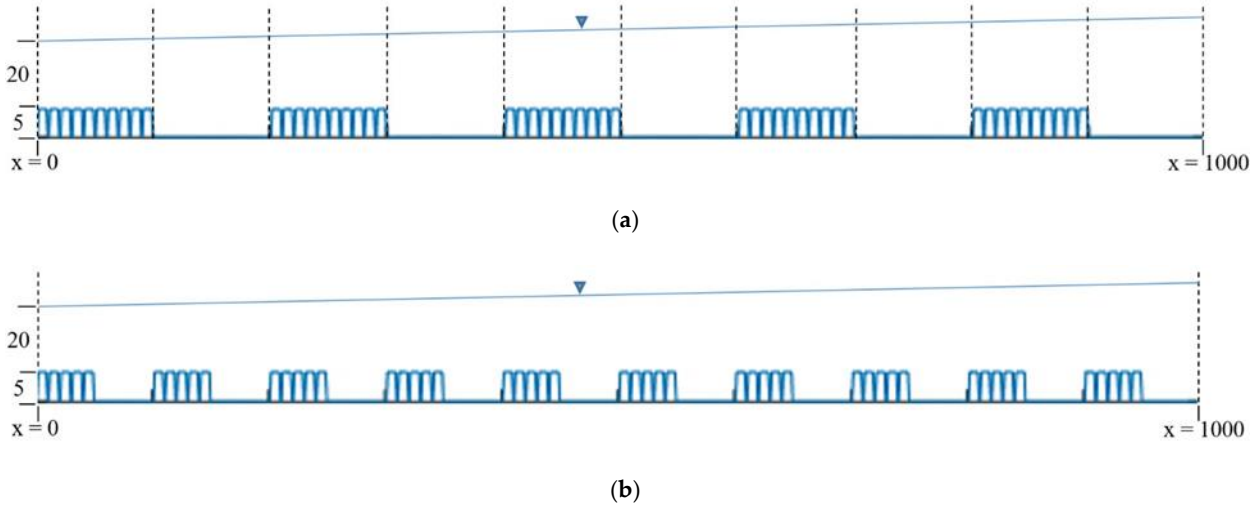


Figure 7. Streambed setups with variation in the extent of gravel and sand portion. Models' setups used for the analysis are zgst5 × 10-5 (**a**), zgst5 × 10-10 (**b**). All units are in mm.

A stream water flow direction (x) of 1 m is considered to be long, as shown in the Figure 8. A constant value of hydraulic conductivity in three directions, $K_{xx} = K_{yy} = K_{zz} = 8.3 \times 10^{-3}$ m/s for gravel and $K_{xx} = K_{yy} = K_{zz} = 3.3 \times 10^{-5}$ m/s for sand was set in the groundwater model [60]. Therefore, a fully saturated groundwater model is the result used for the analysis. The porosity n for calculating the pore water velocity is kept to 0.33, which is a reasonable value for heterogeneous streambed sediments [58]. To simplify the model, the bottom and sides of the groundwater model domain are set as a no flow barrier. The bottom of the domain exists at a depth of 1 m below the bottom of streambed. Due to small scale HH variation resulting from the gravel and sand particles, a small scale hyporheic exchange is expected. This is the reason why the groundwater model dimensions are set as illustrated in Figure 8.

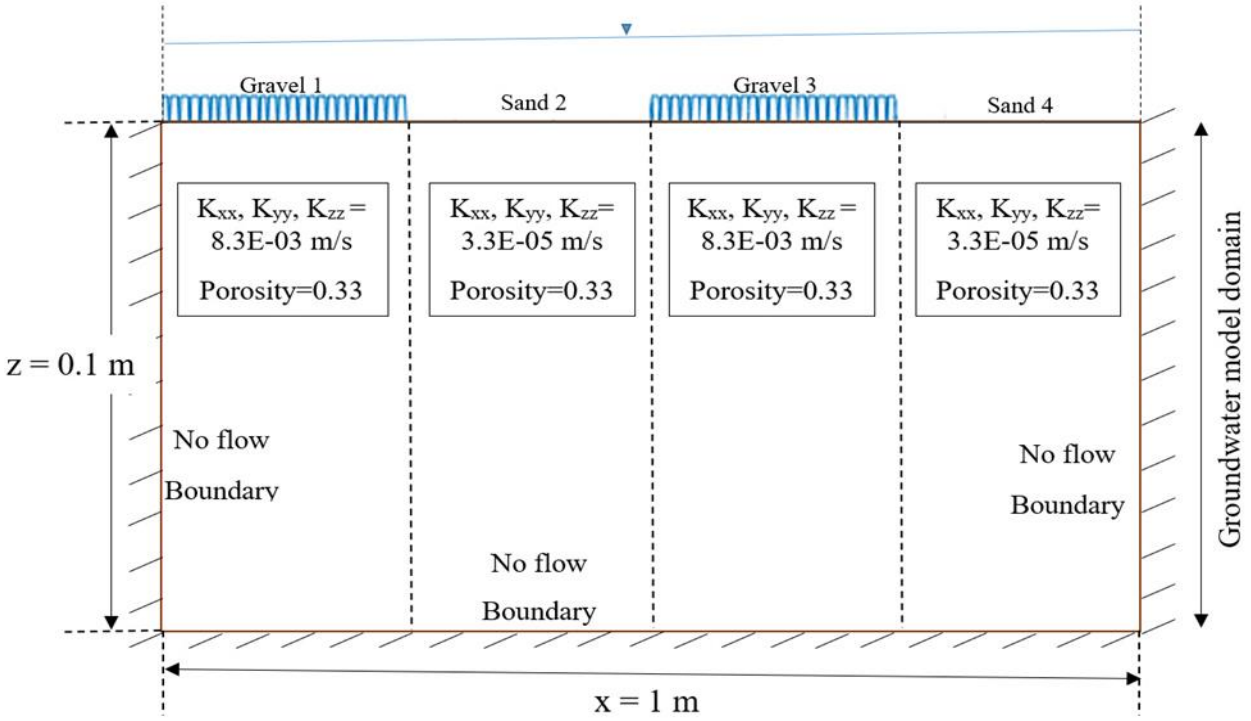


Figure 8. Subsurface water flow model domain with gravel/sand partitioning in streambed and subsurface zone.

2.4. Automated Generation of Hyporheic Streamlines

Required input files of Min3p can be subdivided into problem specific input files. The problem-specific input file is composed of a series of sections or data blocks. Each data block contains specific information of input and may contain a series of sub-sections or sub-blocks for more detailed input information. There are a total of 17 Data blocks in Flow.dat file. The data blocks can appear in any order in the input file, and the order of the subsections within each section can also vary [61].

For tracking particles, a base model is set up using subsurface water flow modelling code MIN3P, which provides an implicit solution to the Richard's equation. A fully saturated porous model domain under steady condition (no temporal variation) was assumed for the analysis [60]. Fully saturated flow condition and steady state simulation was set in data block no. 1 (global control parameters). A three-dimensional computational space was set up based on the dimensions of X:Y:Z = 1:0.1:0.1 m in data block no. 3 ('spatial discretization'). From the upstream and downstream modelling domain, a constant hydraulic head boundaries condition was parameterized by a linear drop in data block no. 13. A different number of control volumes were considered along x, y and z for spatial discretization. For particle tracking, the number of control volume along x, y and z was considered to be 450, 30 and 25, respectively. The units for the output can be specified in years, days, hours, or seconds. The unit of the time step is fixed as hours for this study.

After providing the necessary input data in Flow.dat file, the simulation was run and performed by an automated process using MATLAB. A velocity vector field file was generated after the simulation was run for the whole model domain. Velocity components (v_x, v_y, v_z) at the center of each of the computational cells along with the coordinates (x,y,z) were calculated by Min3p and presented in a text document (.txt). Coordinates of the computational cells and corresponding velocity components were imported and stored in Matlab as variables (x,y,z and v_x, v_y, v_z). The initial condition was defined for fully saturated flow by the hydraulic head. The distribution of this parameter can be discretized across the model domain by means of zones. The initial condition for the zone was set to be 0.1 m. The initial condition was given in terms of the hydraulic head. The zone was specified for the entire solution domain (x = 0 to 1.0, y = 0 to 0.1, z = 0 to 0.1). The number and names of boundary zones, boundary type, boundary value and the extent of the zone are defined in this data block. In this study, four boundary zones, namely, sand1, gravel1, sand2 and gravel2, are defined. The extent of the boundary zones is considered to be x = 0 to 0.25, y = 0 to 0.1 for sand1, x = 0.25 to 0.5, y = 0 to 0.1 for gravel1, x = 0.5 to 0.75, y = 0 to 0.1 for sand2 and x = 0.75 to 1, y = 0 to 0.1 for gravel2. The boundary conditions for sand (sand1 and sand2) and gravel (gravel1 and gravel2) zones are considered to be the first type (Dirichlet) boundary conditions with a value of 0.1 and 0.101 m (hydraulic head or pressure head), respectively. Due to the fact that high hydraulic heads are considered for use in gravel zones, and the water movement inside the model domain, streamlines are therefore expected in these zones in a greater amount.

Numerical Method of Particle Tracking

Particles seeded from the surface of model domain are traced in an automated process using Matlab. Min3p code is used for generating the velocity field file. There are six variables providing the coordinates of the grid points (x, y, z) and the velocity components (v_x, v_y, v_z) in the velocity field file. The velocity field file generated from Min3p is imported in Matlab, keeping only the variables of locations and their corresponding velocities (x, y, z and v_x, v_y, v_z) stored in a 2D array. Several velocity field files, with a required change in the data block of the Min3p code, can be generated and imported within the MATLAB interface with the help of MATLAB Code. Z coordinates of the seeding points were assumed to be fixed as the particle seeding is feasible and realistic from the surface of the model domain and that is the maximum z plane (z = 0.1 m). X and Y coordinates of the seeding points were varied in the z plane.

After getting the particle's seeding location, the program searches the nearest location or asks whether the particle stays exactly on any meshing point (computational nodes generated by Min3p) and the corresponding velocity (stored in computational cell center), RK-4 method is used for the numerical integration of streamlines. The program searches the nearest location of the seeded particle to predict the next location. Using Equation (10), the program determines the next location of the particle. If the particle is seeded exactly at y = 0.1 m, which is the maximum boundary in y direction, the program searches the nearest computational nodes (center of the computational cell), with the nearest y coordinate being y = 0.1 m. The nearest y coordinate in the computational nodes is 0.0991 and can be found by max(y) function in MATLAB from the array storing computational nodes and their corresponding velocities. For example, one of the nearest points of y = 0.1m plane is considered to be (0.6336, 0.0991, 0.0896) and the corresponding velocity field is (-0.0414, 2.1630×10^{-10}, 1.5420). The unit of the velocity is considered to be m/h. The predicted y location of the particle, P_y can be written as, $P_{i+1} = P_i + (1/6)\Delta t\ \vec{v}_i + (1/3)\Delta t\ \vec{v}^{1}_{i+1} + (1/3)\Delta t\ \vec{v}^{2}_{i+1} + (1/6)\Delta t\ \vec{v}^{3}_{i+1}$ and that is $0.1 + 0.0001 \times 2.1630 \times 10^{-10}$, which is slightly greater than the boundary location of y = 0.1 m. This is where the program stops the iteration process and terminates tracing the particle. The inputs of the automated particle tracing program are classified into three categories, such as seeding locations of the particles, boundary of the model domain and the simulation time and time step control.

3. Results

3.1. Hydraulic Head Distribution

Distribution of a hydraulic head over the streambed was generated using a 1D streamflow model and was assigned to the upper boundary condition for the subsurface flow model. High hydraulic gradient was found in the gravel zone and considerably low gradient was found in the sand zone of streambed. Due to the variation in hydraulic head gradients, hyporheic exchange was initiated from the regions of higher hydraulic head with streamlines traveling towards regions with lower hydraulic head. In our case, variations in the hydraulic head were found due to the variation in streambed elevation. High elevations in the streambed with a repetitive ridge and depression pattern were defined for the gavel portion of the bed. Below in Figure 9, change in hydraulic head is shown for the base case scenario (gpt 10×10). The average hydraulic head gradient above the gravel zone, being between x = 0 to x = 0.25 and x = 0.5 to x = 0.75, was found to be 0.005 m/m for base case scenario (gpt10x10). Due to the flat surface with zero slope being defined for the sand zones, the average hydraulic head gradient above these zones was close to zero (0.000082 m/m). Channel roughness was the only reason behind creating the hydraulic head gradient in the sand zone. Small scale changes in hydraulic heads were observed between the individual gravel piece, due to the ridge and depression.

The size of the individual gravel piece has been shown to have a significant impact on the distribution of the hydraulic head. Height and base width were varied to analyze the change in hydraulic head distribution over the entire stream bed. Model setups for the variation in the size of the gravel piece tabulated in the methodology section were considered for the impact analysis. 1D hydraulic head distribution was obtained from HEC-RAS streamflow model simulation. Then, the water surface rises gently over the flat top of the gravel (in case of trapezoidal gravel piece) due to channel roughness. In Figure 10b, region A'A" with gravel piece no. 1, 2 and 3 (red marked) can be observed to understand the phenomena. Due to this change in the water surface elevation, and hence, the hydraulic head, a small scale hyporheic exchange can be expected from the region of the higher hydraulic head to the lower hydraulic head. However, globally, i.e., in the scale of gravel portion (x = 0 to 0.25 m) of the streambed illustrated in Figure 10a, the hydraulic head gradient can be averaged. In this fashion, larger hyporheic exchange, and hence significant HRT, can be achieved.

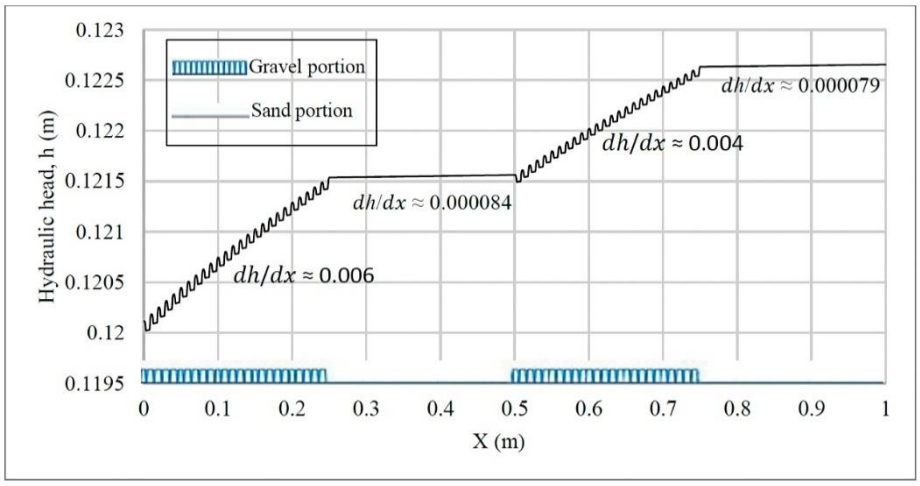


Figure 9. Distribution of hydraulic head over the length of stream bed. The graph above depicts the base case scenario: gpt10 × 10, where the height and base width of gravel piece was 10 m.

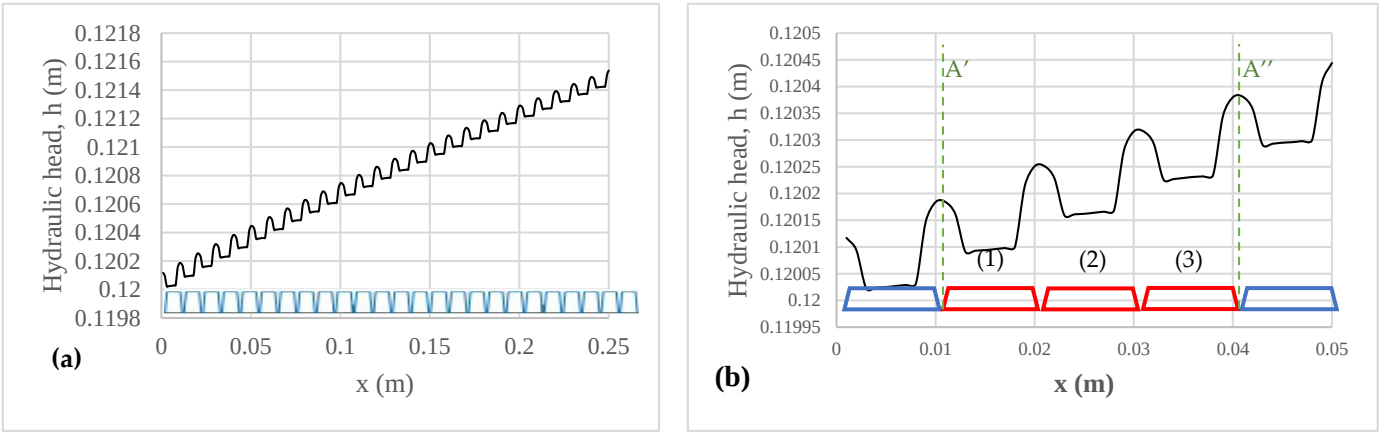


Figure 10. (**a**). Distribution of hydraulic head in the gravel portion (x = 0 to 0.25 m), In (**b**), a zoomed visualization of the change in the hydraulic head from x − 0 to 0.05 m in the scale of the gravel piece (10 mm) (base case).

The size and shape of the gravel piece influence the distribution of hydraulic heads significantly. Streambed elevations are varied to represent the variation in size and shape of gravel pieces. Model setups mentioned in Tables 2 and 3 in the methodology chapter are used to delineate the streambed topology with varying sizes and shapes of gravel pieces. In Figure 11, it can be seen that the hydraulic head increases significantly with an increasing height of an individual gravel piece, whereas it decreases with an increase in the base width of a gravel piece in the streambed. For example, in cases with model setups of gpt5 × 10 and gpt20 × 10, the height of the gravel piece is increased from 5 mm to 20 mm, keeping the base width constant (10 mm). Due to such a change in the height of the gravel pieces, there is a change in the streambed elevation in the gravel portion, and the hydraulic head at location x = 1 m was increased from 0.121 m to 0.141 m, i.e., 0.02 m. On the other hand, in the case of model setups gpt5 × 10 and gpt5 × 25, the base width of the gravel piece was increased from 10 mm to 25 mm, keeping the height constant (5 mm). Hydraulic head at the location x = 1 m was decreased from 0.12088 m to 0.12065 m, i.e., 0.00023 m, which is smaller in order of magnitude.

Table 2. Model setups for the analysis of the effect of base width variation over hyporheic exchange. Units are mm.

Group	Simulation ID/Model Setup	Description
Base width of gravel piece (b_w)	gpt5 × 5	Trapezoidal gravel particle with h = 5, b_w = 5
	gpt5 × 10	Trapezoidal gravel particle with h = 5, b_w = 10
	gpt5 × 25	Trapezoidal gravel particle with h = 5, b_w = 25
	gpt5 × 50	Trapezoidal gravel particle with h = 5, b_w = 50
	gpt5 × 125	Trapezoidal gravel particle with h = 5, b_w = 125
	gpt5 × 250	Trapezoidal gravel particle with h = 5, b_w = 250

Table 3. ID and description of the model setups for the analysis of the effect of variation in distribution of gravel and sand portion over hyporheic exchange.

Group	Simulation ID/Model Setup	Description
Variation in the distribution of gravel and sand portion	zgst5 × 10-2	Sand and gravel zone with trapezoidal gravel piece, h = 5, bw = 10; no. of zone of gravel = 2, no. of zone of sand = 2.
	zgst5 × 10-5	Sand and gravel zone with trapezoidal gravel piece, h = 5, bw = 10; no. of zone of gravel = 5, no. of zone of sand = 5.
	zgst5 × 10-10	Sand and gravel zone with trapezoidal gravel piece, h = 5, bw = 10; no. of zone of gravel = 10, no. of zone of sand = 10.
	zgst5 × 10-20	Sand and gravel zone with trapezoidal gravel piece, h = 5, bw = 10; no. of zone of gravel = 20, no. of zone of sand = 20.
	zgst5 × 10-25	Sand and gravel zone with trapezoidal gravel piece, h = 5, bw = 10; no. of zone of gravel = 25, no. of zone of sand = 25.
	zgst5 × 10-50	Sand and gravel zone with trapezoidal gravel piece, h = 5, bw = 10; no. of zone of gravel = 50, no. of zone of sand = 50.

Groundwater model dimension is considered to be 1:0.1:0.1 m (x:y:z). Longest dimension.

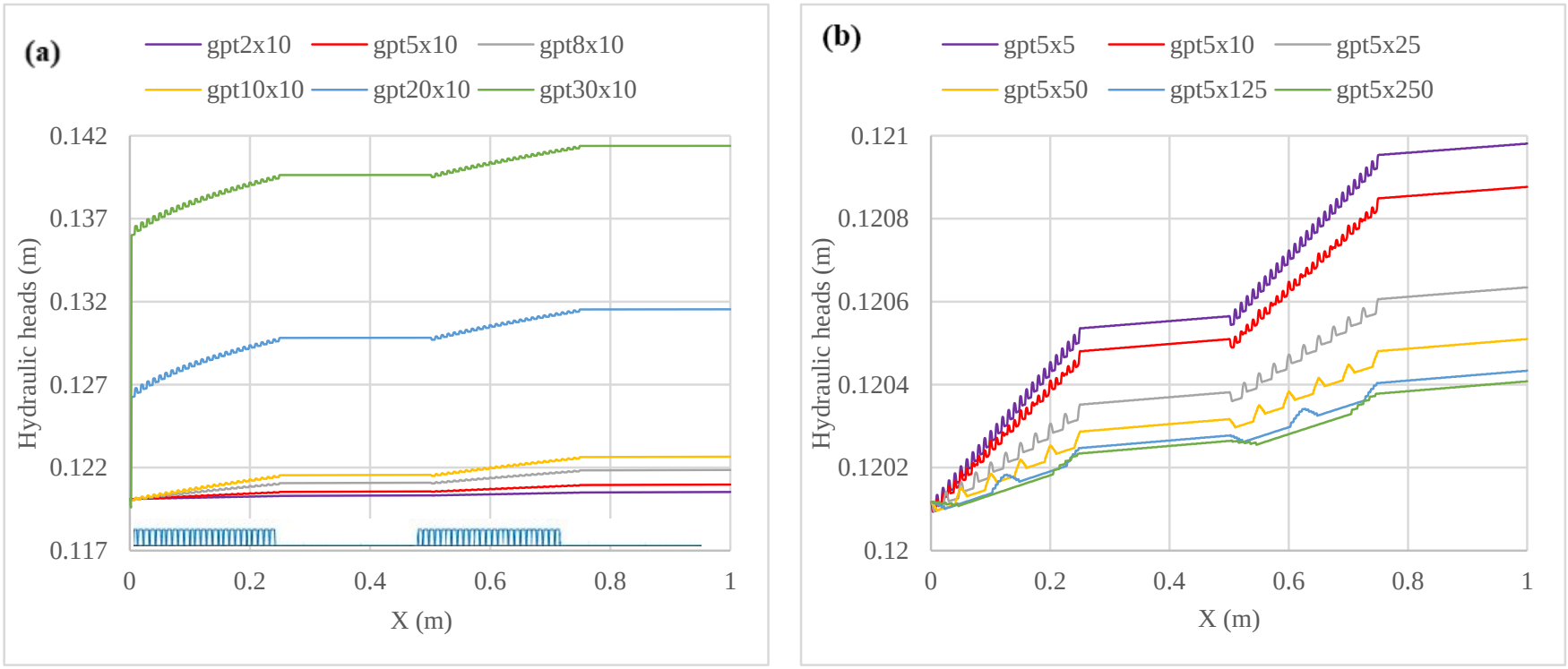


Figure 11. Variation in the distribution of hydraulic head due to a change in the shape of the gravel piece. In (**a**), height of the gravel piece was increased from 2 mm to 30 mm and in (**b**), base width of the gravel piece was increased from 5 mm to 250 mm to observe the change in the hydraulic head distribution.

Hydraulic head gradients (HHG) also varied with the change of gravel size. In Table 4, with the increase in height of the gravel piece, HHG increased in gravel zones, while it decreased in sand zones. Model setups gpt2 × 10, gpt5 × 10, gpt8 × 10, gpt10 × 10, gpt20 × 10 and gpt30 × 10 are used to estimate the change in HHG due to the increase in the height of the gravel piece. On the other hand, model setups gpt5 × 5, gpt5 × 10, gpt5 × 25, gpt5 × 50, gpt5 × 125 and gpt5 × 250 are used to analyze the effect of change in the base width of the gravel piece. In this case, HHG decreased due to an increase in the base width of the gravel piece. Moreover, in the case of sand, the hydraulic head gradient increased.

Table 4. Variation in HHG in the transition zones of gravel and sand portion of the streambed.

Simulation ID	Zone of Stream Bed			
	Gravel1	**Sand2**	**Gravel3**	**Sand4**
gpt2 × 10	0.000177	0.000029	0.000172	0.000029
gpt5 × 10	0.000419	0.000029	0.000388	0.000028
gpt8 × 10	0.000946	0.000027	0.000747	0.000024
gpt10 × 10	0.001420	0.000025	0.001071	0.000021
gpt20 × 10	0.009697	0.000009	0.001708	0.000008
gpt30 × 10	0.019511	0.000004	0.001750	0.000003
gpt5 × 5	0.000419	0.000029	0.000388	0.000028
gpt5 × 10	0.000364	0.000029	0.000339	0.000028
gpt5 × 25	0.000235	0.000029	0.000224	0.000028
gpt5 × 50	0.000170	0.000030	0.000164	0.000029
gpt5 × 125	0.000130	0.000030	0.000127	0.000030
gpt5 × 250	0.000117	0.000030	0.000114	0.000030

In Figure 12, the difference in HHGs of four zones with the increase in the size of the gravel piece are shown. In Figure 12a, the effect of increasing the height of the gravel piece is illustrated. It can be observed that the difference in HHGs is increased with the increase in height. The increase in zone 1 and 2 (gravel 1 and sand 2) is much higher than the increase in zone 3 and 4 (gravel 3 and sand 4). However, in a case where there is a change in the base width of the gravel piece, the behavior of HHGs is observed to be the opposite. With an increase in the base width of the gravel piece, the difference in the HHGs also decreases. Both the increase and decrease in HHG are approximately exponential in nature.

From the above investigations it can be said that due to the rise in the height of the gravel piece, HH distribution and HHG increase. On the other hand, an increase in the base width of the gravel piece causes the HH and HHG to be decreased. The change in HH, and hence HHG, is the most important driver for hyporheic exchange and have a major impact on HRT. The impact on hyporheic streamline distribution and HRT are discussed in the later section.

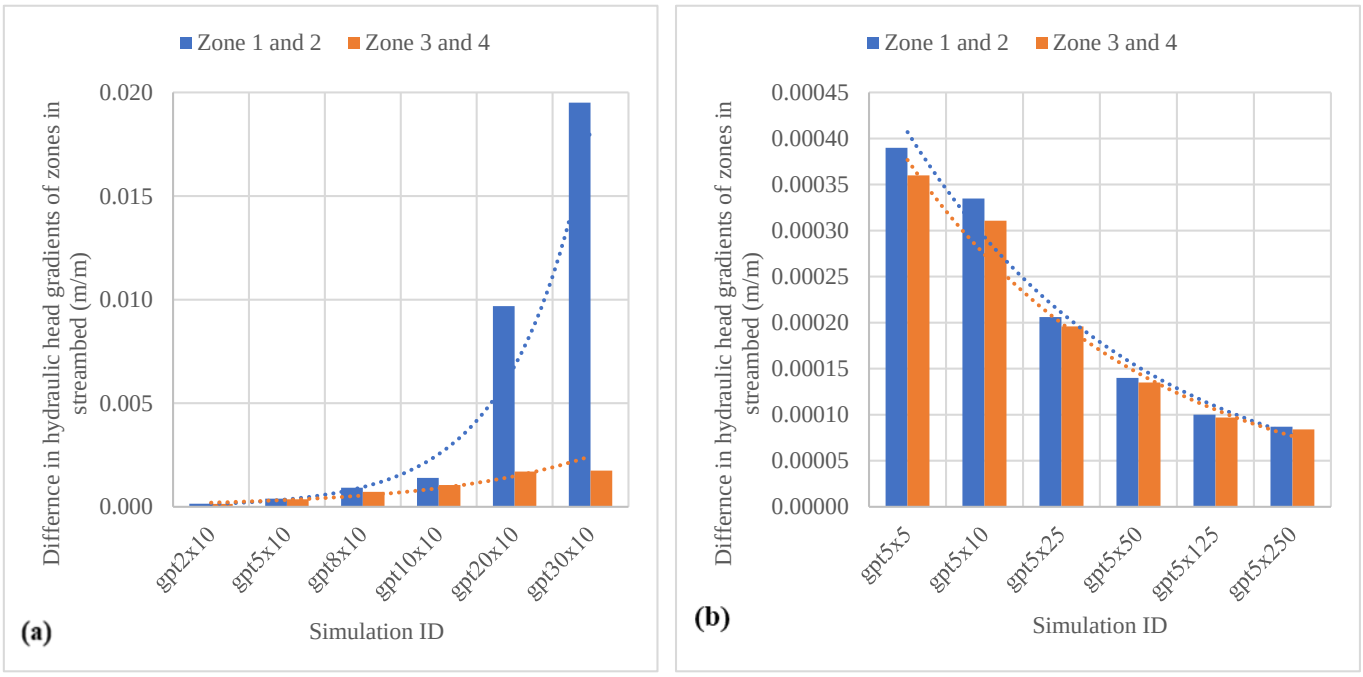


Figure 12. Change in the difference in HHGs of four zones with gravel and sand in the streambed with increasing height (**a**) and base width (**b**) of gravel pieces. Explanation of model setups can be found in the methodology chapter.

3.2. Subsurface Flow Field

Velocity vector field is generated in MIN3P by solving the saturated subsurface flow equation. Velocity vector components (v_x, v_y, v_z) are derived and stored at every computational node (x,y,z). In total, 196,000 nodes are generated to create a velocity vector field for a subsurface model of the base case (gpt10 × 10). The values of vx and vz have larger values compared to vy (see Table 5). This is due no variation in hydraulic head distribution being considered in y direction. The numerical value of the mean and standard deviation is mentioned in the Table 5. The mean of vx is found to be negative, where the mean of vy and vz are found to be positive. A positive value of vz shows upwelling velocity component, which is a crucial factor for hyporheic exchange. However, due to the high value of Standard Deviation, considering the mean only represents a general overview of the velocity vector field and is not satisfactory.

Table 5. Average (mean) value and standard deviation of the velocity components.

Mean (μ) (m/h)			**Standard Deviation (σ) (m/h)**		
v_x	v_y	v_z	v_x	v_y	v_z
−6.424	1.212×10^{-8}	7.1861×10^{-5}	13.845	3.061×10^{-8}	7.966

The mean value of v_x, v_y, v_z does not represent the whole vector field as the value of the other elements of v_x, v_y, and v_z deviate significantly over a wide range. The variations in the vector components along x and z are higher than the vector components along y direction. The v_x and v_z are of particular importance as they are responsible for contributing the streamlines down in the subsurface model domain. Velocity component along y direction were found to be negligible

Hydraulic head gradient in gravel portions are high compared to sand portions and causes diversified velocity field where in the sand portion, this field remains too small. Large HHGs are created due to high hydraulic head values, which are directly linked to the streambed elevation. Therefore, it can be said that the size of the particle in the channel bed

is a determining factor for creating a mixture of upwelling (+ve) and downwelling (-ve) velocity components and, consequently, for creating hyporheic exchange. In Figure 13, the effect of the change in size of the gravel piece on the mean, range and SD of velocity vector field are shown. Model setups gpt2 × 10, gpt5 × 10, gpt8 × 10, gpt10 × 10, gpt20 × 10 and gpt30 × 10 are used to analyze the effect of increasing height of gravel pieces. With the increase in height of the gravel pieces, the mean, range and SD also increases. This behavior indicates that the absolute values and spread of velocity vector field are increased with the increase in height of gravel. On the other hand, mean, range and SD of the velocity field decreased with increasing base width of gravel. Therefore, the absolute values and spread of velocity vector field are decreased with the increase in base width of the gravel piece.

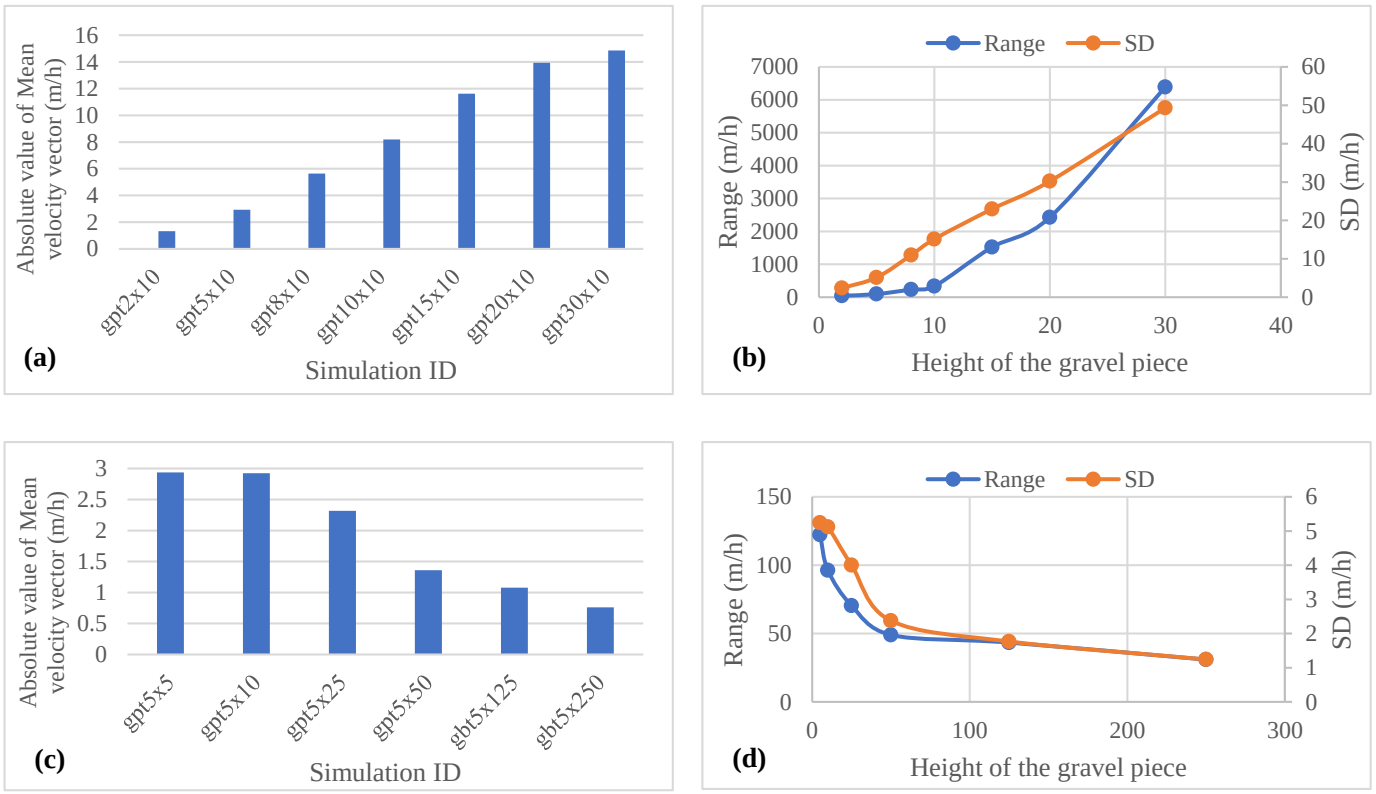


Figure 13. Effect of change in the height (**a**,**b**) and base width (**c**,**d**) of gravel piece on the velocity vector field. Mean, range, and SD are shown to compare the impact of varying gravel size.

3.3. Hyporheic Streamline Distribution

Model setups used for investigation of the effect of variation in height of gravel pieces can be seen in Table 1 of methodology chapter. Distribution of gravel and sand portion of the channel band are kept alternatively, one after another, at a 250 mm distance. The base width of each gravel piece in gravel portion of the channel bed are kept a constant 10 mm. In Figure 14a,b, distribution of streamlines due to height variation can be observed. It is clear from the figure that the number of streamlines generated from the particles seeded from the surface of the model domain increases with the rise in the height of the gravel piece. Besides the larger streamlines generated from the transition zone of gravel and sand portion of the streambed to the middle of the sand portion, some smaller streamlines are generated in the gravel zone.

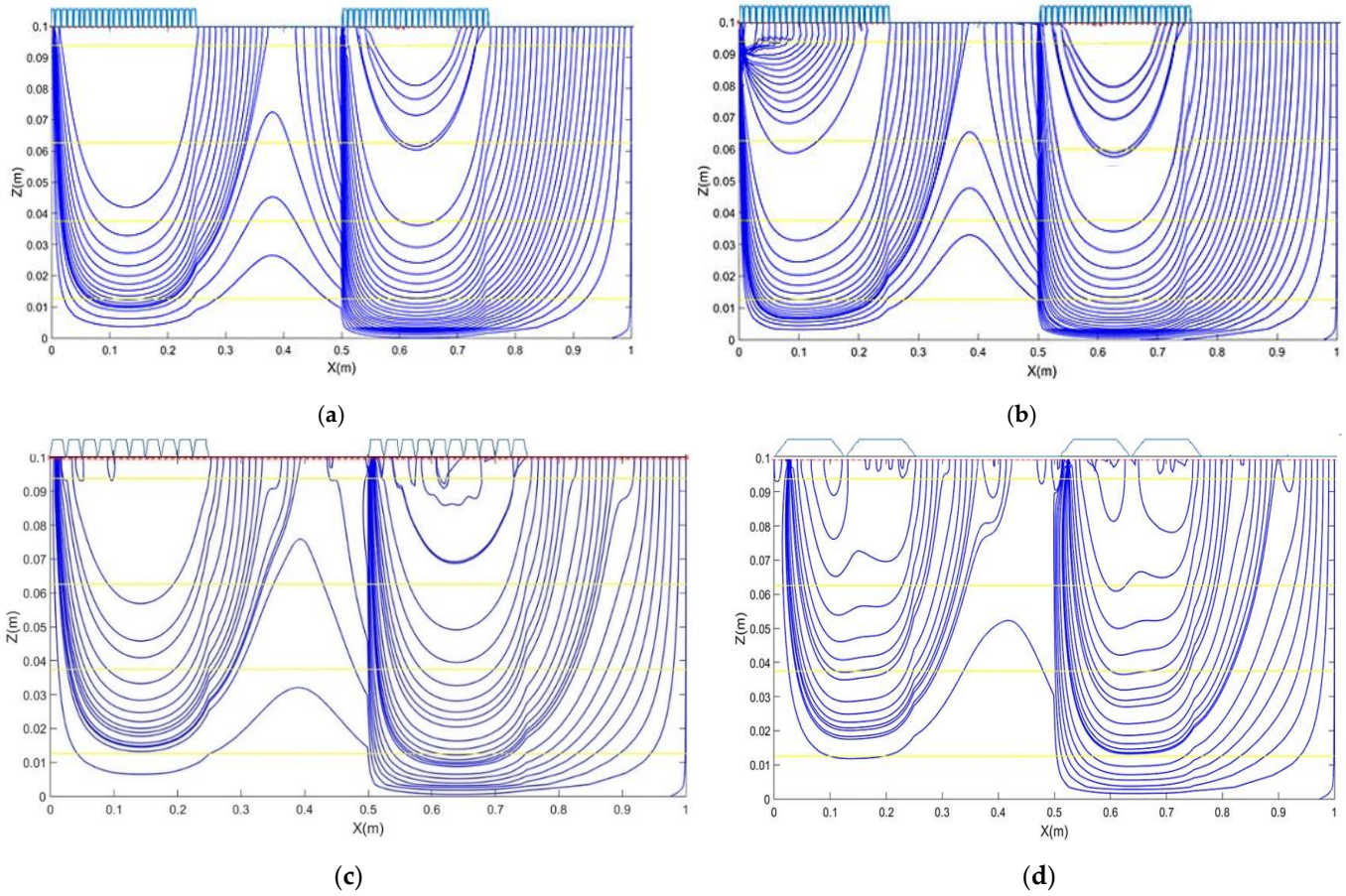


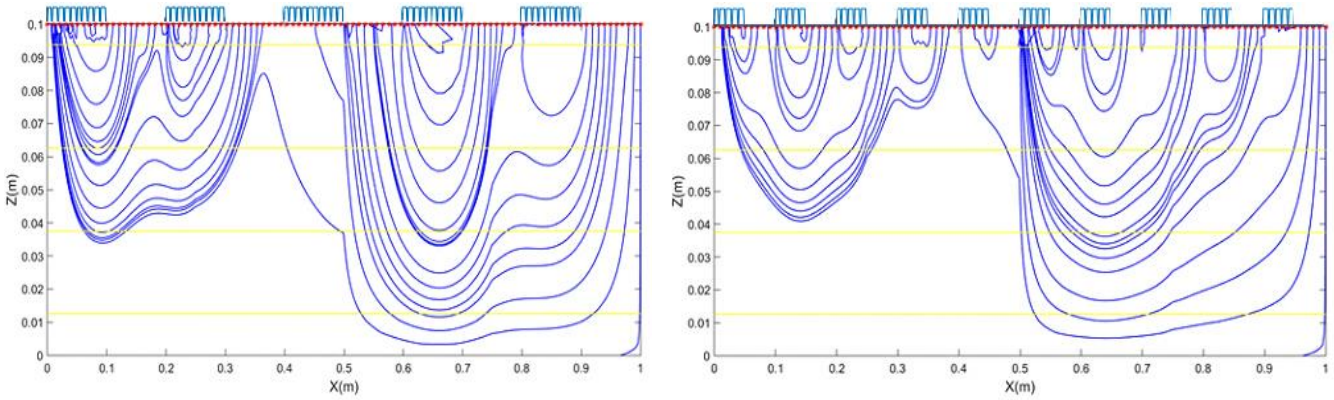
Figure 14. Distribution of streamlines for model set ups gpt8 × 10 (**a**) and gpt30 × 10 (**b**). Height variation in gravel pieces influences the number of streamlines generated from the same seeding locations. Gravel portions were shown using a rectangular block on the top of the figure distribution of streamlines for model set ups gpt5 × 25 (**c**), and gpt5 × 125 (**d**) resulted from the variation in base width of the gravel piece.

This is due to the fact that gravel pieces with greater height induce high hydraulic head and thus create higher downwelling and upwelling velocity fields, which are the driving force of hyporheic exchange. Moreover, a 1 mm gap was assumed between the gravel pieces, which also causes a rise and fall in hydraulic head together with the top of the gravel piece. The length of the streamline also increases with the increase in height of gravel piece. Longer and wavy streamlines are found in sand4 zone where the streamlines generated and ended at gravel1 zone. Consequently, these streamlines needed more time to travel, and hence, they resulted in high HRT.

On the other hand, model setups used for the investigation of the effect of variation in base width Figure 14c,d of gravel pieces are gpt5 × 5, gpt5 × 10, gpt5 × 25, gpt5 × 50, gpt5 × 125 and gpt5 × 250 where the base width of gravel pieces is varied from 5 to 250 mm. In case of variation in base width of gravel pieces, an overall change in the distribution of streamlines can be observed in Figure 14. The length of the streamlines was reduced, whereas the number of streamlines was increased with the increase in the base width. Compared to the case of height variation, the number of small streamlines was increased. The shape of the streamlines of model setups gpt5 × 125 and gpt5 × 250 became wavier compared to the models' setups gpt5 × 5, gpt5 × 10, gpt5 × 25 and gpt5 × 50. In this case, as with the case of height variation, longer streamlines are observed in the sand1 zone where the model boundary ends and no influx or outflux were considered.

In both cases, the total number of streamlines was observed to have increased due to increase in height and base width of an individual gravel piece, where the shape and length of streamlines differed.

Model setups used for investigation of the effect of variation in the distribution of gravel pieces are zgst5 × 10-2, zgst5 × 10-5, zgst5 × 10-10, zgst5 × 10-20, zgst5 × 10-25 and zgst5 × 10-50. Detail of the model setups used can be seen in Table 4 of methodology chapter. Dramatic variation in the distribution of streamlines can be observed due to change in the distribution of gravel and sand portion over the channel bed. With the increase in the number of gravel and sand portions, number of streamlines reduces (see Figure 15a,b). Moreover, the length of streamlines also declines. Streamlines become more narrow and smaller with the increase in gravel and segments. In the case of model setup zgst5 × 10-50, where 50 segments of gravel and sand are set up, most of the streamlines are found to be smaller and the number of streamlines decrease significantly.



(**a**) (**b**)

Figure 15. Distribution of streamlines for model set ups zgst5 × 10-5 (**a**), zgst5 × 10-50 (**b**). The figure illustrates the effect of change in distribution of gravel and sand portion of streambed over streamline distribution.

3.4. Residence Time

Size (height and base width) of an individual gravel piece was altered to analyze the impact over HRT distribution. Due to the varying hydraulic head distribution, velocity vector field of the subsurface model domain varies and hence the change in HRT distribution occurs. HRTs were observed to be increased with the increase in base width of gravel piece (see Figure 16).

Distribution of HRT for the model setups zgst5 × 10-5, zgst5 × 10-25, are shown in Figure 17a,b, respectively, where the outcomes of the variation in the distribution of gravel and sand portion are illustrated. A decreasing trend in HRT is observed with the increase in the number of gravel/sand zones.

A decreasing trend is observed in mean residence time with an increasing number of particles seeded from the surface. Mean residence time is measured over the whole x horizon (x = 0 to x = 1) at y = 0.05 and z = 0.1 using base case scenario. Zone from x = 0.25 to x = 0.5 and x = 0.75 to x = 1 constitute streamlines thus approximately 50% of the whole model domain constitutes the streamline. The means residence time reached 6.924 h from 7.7872 h when the seeding location increased from 50 to 2000 and obtained a stable condition, where the mean residence time does not change considerably with the increase in seeding location in Figure 18.

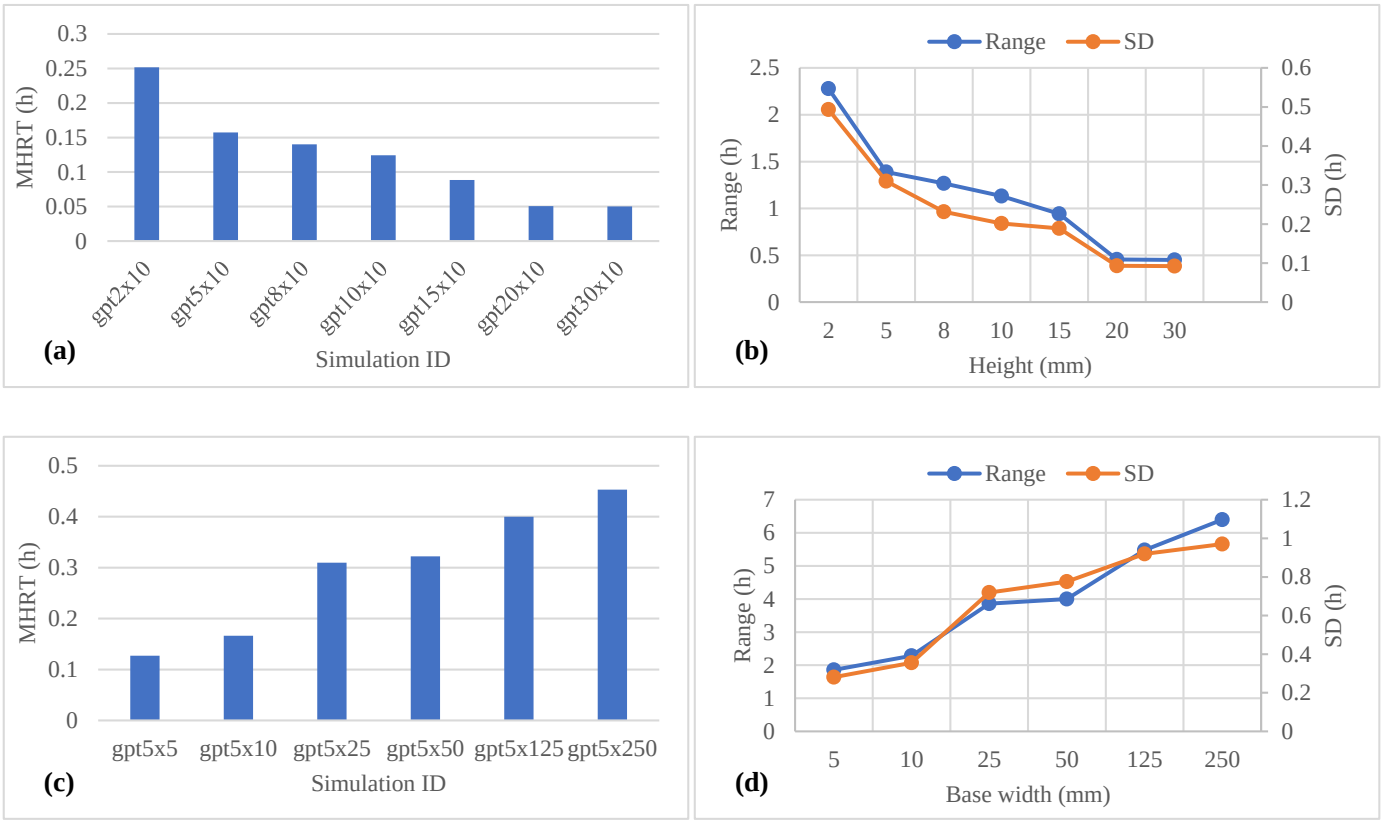


Figure 16. Impact of the size of gravel particle on mean, range, and SD of HRT. Due to an increase in the height of gravel pieces in the figure (**a**,**b**), mean, range and SD of HRT decreases. On the other hand, with the increase in the base width of gravel pieces in the figure (**c**,**d**), these values increase.

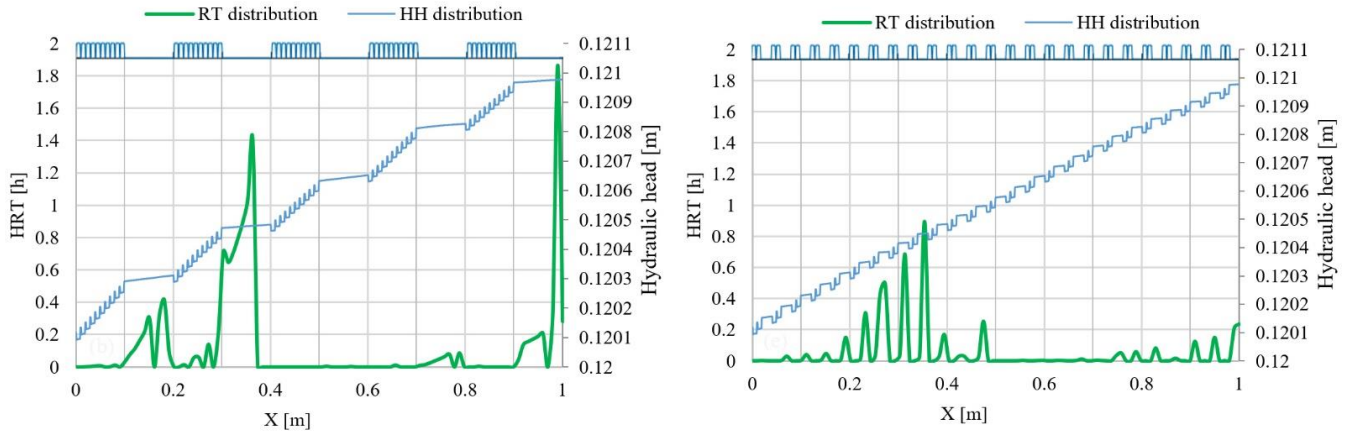


Figure 17. Variation in HRT is shown with the change of distribution of gravel-sand portion in streambed. Model setups zgst5 × 10-5 (**a**) and zgst5 × 10-25 (**b**) are used to compute the HRT distribution.

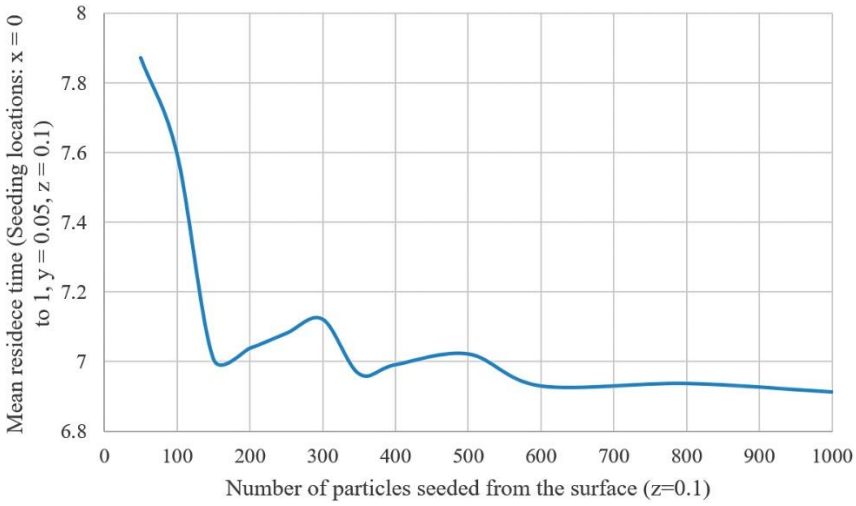


Figure 18. Variation of the mean residence time with the change in number of particles seeded from the model surface.

4. Conclusions

In the streambed created with gravel and sand, variation in elevation is brought by the size, shape, and change in the distribution of gravel and sand segments. These parameters are varied within a certain range to observe the response of hyporheic exchange. Due to the change in streambed elevation occurring in such a way, hydraulic head distribution is altered. Surface water modeling software, HEC-RAS, is used to generate and store the alterations in the hydraulic head distribution in response to the change in channel elevation. In the case of an increase in height of a gravel piece, hydraulic heads increase as well. A contrary scenario was detected in cases with an increase in the base width of a gravel piece. A similar situation was observed in cases with a variation in the number of gravel-sand segments. However, change in the shape of a gravel piece did not show significant variation in hydraulic head distribution compared to the other cases.

Consequently, a change in the subsurface flow field occurred as the hydraulic heads obtained from surface water analysis were used as the boundary condition of the subsurface computational space. Due to a change in streambed geometry, a large deviation in flow field was monitored. The velocity vector fields that resulted due to this change showed a large spread of values where the mean of velocities did not represent the flow field at all. With the increase in hydraulic head values, the spread and mean value of flow fields increased. In this flow field generated in the groundwater model domain, streamlines were generated from predetermined uniformity distributed seeding locations. The distribution of streamlines that resulted from the different flow field was found to be sensitive to the change in streambed geometry. The number and length of streamlines varied significantly in response to a change in hydraulic head distribution, and thus, a change in the size, shape, and number of segments.

Finally, higher residence times were found where the hydraulic head values were lower. In cases with an increasing height of gravel piece where the hydraulic head values were increasing, HRTs were smaller. Conversely, where there was a lower hydraulic head, HRT was higher. For instance, in cases with an increasing base width of the gravel pieces where hydraulic head values were lower, HRT s were found to be greater. Moreover, some small scale HRTs and streamlines were found in cases with a high number of gravel-sand segments.

In a concluding remark, it can be said that the stream bed morphology, hydraulic heads over the subsurface domain, flow field in the subsurface, and lastly, the hyporheic exchange, are all interlinked and should be examined together. Ignoring the effect of one of them may lead to an erroneous prediction of hyporheic exchange. Further assessment of the linkage among them to build a powerful mathematical relationship alongside the use of more broad and high-resolution data are highly recommended.

Author Contributions: Conceptualization, M.A.A.M.; Methodology, M.A.A.M. and M.M.S.Y.; Investigation, M.A.A.M. and M.M.S.Y.; Formal Analysis, M.A.A.M. and M.M.S.Y.; Resources, M.A.A.M.; Data Preparation, M.A.A.M.; Writing—Original Draft Preparation, M.A.A.M., M.M.S.Y., W.A., M.T.A., R.K. and A.R.; Writing—Review and Editing, W.A., M.T.A., R.K. and A.R.; Visualization M.A.A.M. and M.M.S.Y.; and Project Administration, M.A.A.M. All authors have read and agreed to the published version of the manuscript.

Funding: This research received no external funding.

Institutional Review Board Statement: Not applicable.

Data Availability Statement: Data collected for the study can be made available upon request from the corresponding author.

Conflicts of Interest: The authors declare no conflict of interest.

References

1. Kuriata-Potasznik, A.; Szymczyk, S.; Bęś, A.; Sidoruk, M.; Skwierawski, A.; Kobus, S. Role of River–Lake System Sediments and Microbial Activity in the Hyporheic Zone. *Water* **2021**, *13*, 3499. [CrossRef]
2. Nawalany, M.; Sinicyn, G.; Grodzka-Łukaszewska, M.; Mirosław-Świątek, D. Groundwater–Surface Water Interaction—Analytical Approach. *Water* **2020**, *12*, 1792. [CrossRef]
3. Yazdan, M.M.S.; Ahad, M.T.; Jahan, I.; Mazumder, M. Review on the Evaluation of the Impacts of Wastewater Disposal in Hydraulic Fracturing Industry in the United States. *Technologies* **2020**, *8*, 67. [CrossRef]
4. Fleckenstein, J.H.; Krause, S.; Hannah, D.M.; Boano, F. Groundwater-surface water interactions: New methods and models to improve understanding of processes and dynamics. *Adv. Water Res.* **2010**, *33*, 1291–1295. [CrossRef]
5. Stanford, J.A.; Ward, J.V. The hyporheic habitat of river ecosystems. *Nature* **1998**, *335*, 64–66. [CrossRef]
6. Bencala, K.E. Hyporheic Exchange Flows. In *Encyclopedia of Hydrological Sciences v.3*; Anderson, M.G., McDonnell, J., Eds.; John Wiley & Sons: Hoboken, NJ, USA, 2005; pp. 1733–1740.
7. Al Mehedi, M.A.; Reichert, N.; Molkenthin, F. Sensitivity Analysis of Hyporheic Exchange to Small Scale Changes In Gravel-Sand Flumebed Using A Coupled Groundwater-Surface Water Model (*No. EGU2020-20319*). *Copernic. Meet.* 2020. Available online: https://meetingorganizer.copernicus.org/EGU2020/EGU2020-20319.html (accessed on 13 February 2022).
8. Thomle, J.; Strickland, C.; Johnson, T.C.; Zhu, Y.; Stegen, J. A Flux Detection Probe to Quantify Dynamic Groundwater-Surface Water Exchange in the Hyporheic Zone. *Groundwater* **2020**, *58*, 892–900. [CrossRef]
9. Esteve-Llorens, X.; Ita-Nagy, D.; Parodi, E.; González-García, S.; Moreira, M.T.; Feijoo, G.; Vázquez-Rowe, I. Environmental footprint of critical agro-export products in the Peruvian hyper-arid coast: A case study for green asparagus and avocado. *Sci. Total Environ.* **2021**, *818*, 151686. [CrossRef]
10. Al Mehedi, M.A.; Smith, V.; Hosseiny, H.; Jiao, X. Unraveling the Complexities of Urban Flood Hydraulics through AI. 2022. Available online: https://assets.researchsquare.com/files/rs-1602023/v1/17edf6de-a4df-4859-93b8-bbb55b7ce510.pdf?c=1652287364 (accessed on 13 February 2022).
11. Hordon, R.M. *Hydrological Cycle*; Herschy, R.W., Fairbridge, R.W., Eds.; Encyclopedia of Hydrology and Water Resources; Springer: Dordrecht, Switzerland, 1998; pp. 367–371. Available online: https://link.springer.com/referencework/10.1007/1-4020-4497-6 (accessed on 13 February 2022).
12. Jekatierynczuk-Rudczyk, E.; Puczko, K.; Żukowska, J.; Sawicka, A. Biota communities influence on nutrients circulation in hyporheic zone—a case study in urban spring niches in Bialystok (NE Poland). *Aquat. Sci.* **2021**, *83*, 75. [CrossRef]
13. Uddin, M.G.; Nash, S.; Olbert, A.I. A review of water quality index models and their use for assessing surface water quality. *Ecol. Indic.* **2021**, *122*, 107218. [CrossRef]
14. Shen, G.; Yuan, J.; Phanikumar, M.S. Quantifying the effects of bed roughness on transit time distributions via direct numerical simulations of turbulent hyporheic exchange. *Water Resour. Res.* **2022**, *58*, e2021WR030503. [CrossRef]
15. Yazdan, M.M.; Ahad, M.T.; Mallick, Z.; Mallick, S.P.; Jahan, I.; Mazumder, M. An Overview of the Glucocorticoids' Pathways in the Environment and Their Removal Using Conventional Wastewater Treatment Systems. *Pollutants* **2021**, *1*, 141–155. [CrossRef]
16. Di Lorenzo, T.; Fiasca, B.; Di Cicco, M.; Cifoni, M.; Galassi, D.M. Taxonomic and functional trait variation along a gradient of ammonium contamination in the hyporheic zone of a Mediterranean stream. *Ecol. Indic.* **2021**, *132*, 108268. [CrossRef]
17. Karan, S.; Jacobsen, M.; Kazmierczak, J.; Reyna-Gutiérrez, J.A.; Breum, T.; Engesgaard, P. Numerical Representation of Groundwater-Surface Water Exchange and the Effect on Streamflow Contribution Estimates. *Water* **2021**, *13*, 1923. [CrossRef]
18. Liang, D.; Song, J.; Xia, J.; Chang, J.; Kong, F.; Sun, H.; Cheng, D.; Zhang, Y. Effects of heavy metals and hyporheic exchange on microbial community structure and functions in hyporheic zone. *J. Environ. Manag.* **2022**, *303*, 114201. [CrossRef]
19. Conant, B.; Robinson, C.E.; Hinton, M.J.; Russell, H.A.J. A framework for conceptualizing groundwater-surface water interactions and identifying potential impacts on water quality, water quantity, and ecosystems. *J. Hydrol.* **2019**, *574*, 609–627. [CrossRef]
20. Van Genuchten, M.T. A comparison of numerical solutions of the one-dimensional unsaturated—saturated flow and mass transport equations. *Adv. Water Resour.* **1982**, *5*, 47–55. [CrossRef]

21. Feng, J.; Liu, D.; Liu, Y.; Li, Y.; Li, H.; Chen, L.; Xiao, J.; Liu, J.; Dong, J. Hyporheic exchange due to in-stream geomorphic structures. *J. Freshw. Ecol.* **2022**, *37*, 221–241. [CrossRef]
22. Dibyanshu, K.; Chhaya, T.; Raychoudhury, T. A review on the fate and transport behavior of engineered nanoparticles: Possibility of becoming an emerging contaminant in the groundwater. *Int. J. Environ. Sci. Technol.* **2022**, 1–24. [CrossRef]
23. Salehin, M.; Packman, A.I.; Paradis, M. Hyporheic exchange with heterogeneous streambeds: Laboratory experiments and modeling. *Water Resour. Res.* **2004**, *40*. Available online: https://agupubs.onlinelibrary.wiley.com/doi/full/10.1029/2003WR002567 (accessed on 13 February 2022). [CrossRef]
24. Brunke, M.; Gonser, T.O.M. The ecological significance of exchange processes between rivers and groundwater. *Freshw. Biol.* **1997**, *37*, 1–33. [CrossRef]
25. Haque, A.; Salama, A.; Lo, K.; Wu, P. Surface and Groundwater Interactions: A Review of Coupling Strategies in Detailed Domain Models. *Hydrology* **2021**, *8*, 35. [CrossRef]
26. Wallace, C.D.; Soltanian, M.R. Surface water-groundwater exchange dynamics in buried-valley aquifer systems. *Hydrol. Processes* **2021**, *35*, e14066. [CrossRef]
27. Ikard, S.J.; Briggs, M.A.; Lane, J.W. Investigation of Scale-Dependent Groundwater/Surface-water Exchange in Rivers by Gradient Self-Potential Logging: Numerical Modeling and Field Experiments. *J. Environ. Eng. Geophys.* **2021**, *26*, 83–98. [CrossRef]
28. Boano, F.; Revelli, R.; Ridolfi, L. Bedform-induced hyporheic exchange with unsteady flows. *Adv. Water Resour.* **2007**, *30*, 148–156. [CrossRef]
29. Cardenas, M.B.; Wilson, J.L. Dunes, turbulent eddies, and interfacial exchange with permeable sediments. *Water Resour. Res.* **2007**, *43*. [CrossRef]
30. Cardenas, M.B.; Wilson, J.L. Hydrodynamics of coupled flow above and below a sediment–water interface with triangular bedforms. *Adv. Water Resour.* **2007**, *30*, 301–313. [CrossRef]
31. Magliozzi, C.; Grabowski, R.; Packman, A.I.; Krause, S. Scaling down hyporheic exchange flows: From catchments to reaches. *Hydrol. Earth Syst. Sci.* **2017**, 1–53.
32. Packman, A.I.; Salehin, M.; Zaramella, M. Hyporheic exchange with gravel beds: Basic hydrodynamic interactions and bedform-induced advective flows. *J. Hydraul. Eng.* **2004**, *130*, 647–656. [CrossRef]
33. Smith, J.W.N. Groundwater–Surface Water Interactions in the Hyporheic Zone, Environment Agency. *Sci. Rep.* **2005**, *21*, 13943–13955. [CrossRef]
34. Wilhelmsen, K.; Sawyer, A.H.; Marshall, A.; McFadden, S.; Singha, K.; Wohl, E. Laboratory Flume and Numerical Modeling Experiments Show Log Jams and Branching Channels Increase Hyporheic Exchange. *Water Resour. Res.* **2021**, *57*, e2021WR030299. [CrossRef]
35. Boulton, A.J.; Findlay, S.; Marmonier, P.; Stanley, E.H.; Valett, H.M. The functional significance of the hyporheic zone in streams and rivers. *Annu. Rev. Ecol. Syst.* **1998**, *29*, 59–81. [CrossRef]
36. Frey, S.K.; Miller, K.; Khader, O.; Taylor, A.; Morrison, D.; Xu, X.; Berg, S.J.; Hwang, H.-T.; Sudicky, E.A.; Lapen, D.R. Evaluating landscape influences on hydrologic behavior with a fully-integrated groundwater—Surface water model. *J. Hydrol.* **2021**, *602*, 126758. [CrossRef]
37. Cardenas, M.B.; Wilson, J.L.; Haggerty, R. Residence time of bedform-driven hyporheic exchange. *Adv. Water Resour.* **2008**, *31*, 1382–1386. [CrossRef]
38. Shrivastava, S.; Stewardson, M.J.; Arora, M. Influence of Bioturbation on Hyporheic Exchange in Streams: Conceptual Model and Insights from Laboratory Experiments. *Water Resour. Res.* **2021**, *57*, e2020WR028468. [CrossRef]
39. Tonina, D.; Buffington, J.M. Hyporheic exchange in mountain rivers I: Mechanics and environmental effects. *Geogr. Compass* **2009**, *3*, 1063–1086. [CrossRef]
40. Gatel, L.; Lauvernet, C.; Carluer, N.; Weill, S.; Paniconi, C. Sobol Global Sensitivity Analysis of a Coupled Surface/Subsurface Water Flow and Reactive Solute Transfer Model on a Real Hillslope. *Water* **2020**, *12*, 121. [CrossRef]
41. Cremeans, M.M.; Devlin, J.F.; McKnight, U.S.; Bjerg, P.L. Application of new point measurement device to quantify groundwater-surface water interactions. *J. Contam. Hydrol.* **2018**, *211*, 85–93. [CrossRef] [PubMed]
42. Bencala, K.E. Simulation of solute transport in a mountain pool-and-riffle stream with a kinetic mass transfer model for sorption. *Water Resour. Res.* **1983**, *19*, 732–738. [CrossRef]
43. Blanco-Coronas, A.M.; López-Chicano, M.; Calvache, M.L.; Benavente, J.; Duque, C. Groundwater-Surface Water Interactions in "La Charca de Suárez" Wetlands, Spain. *Water* **2020**, *12*, 344. [CrossRef]
44. Martone, I.; Gualtieri, C.; Endreny, T. Characterization of Hyporheic Exchange Drivers and Patterns within a Low-Gradient, First-Order, River Confluence during Low and High Flow. *Water* **2020**, *12*, 649. [CrossRef]
45. Vaux, W.G. Interchange of stream and intragravel water in a salmon spawning riffle. *U.S. Fish Wildl. Serv. Spec. Sci. Rep. Fish.* **1962**, *405*, 11.
46. Mantey, J.; Nyarko, K.B.; Owusu-Nimo, F.; Awua, K.A.; Bempah, C.K.; Amankwah, R.K.; Akatu, W.E.; Appiah-Effah, E. Mercury contamination of soil and water media from different illegal artisanal small-scale gold mining operations (galamsey). *Heliyon* **2020**, *6*, 4312. [CrossRef] [PubMed]
47. Mantey, J.; Nyarko, K.B.; Owusu-Nimo, F.; Awua, K.A.; Bempah, C.K.; Amankwah, R.K.; Akatu, W.E.; Appiah-Effah, E. Influence of illegal artisanal small-scale gold mining operations (galamsey) on oil and grease (O/G) concentrations in three hotspot assemblies of Western Region, Ghana. *Environ. Pollut.* **2020**, *263*, 114251. [CrossRef] [PubMed]

48. Laube, G.; Schmidt, C.; Fleckenstein, J.H. A systematic model-based evaluation of the influence of hydraulic conductivity, heterogeneity and domain depth on hyporheic nutrient transformation. *Adv. Water Resour.* **2022**, *159*, 104087. [CrossRef]
49. HEC-RAS Manual. Available online: https://www.hec.usace.army.mil/software/hec-ras/documentation.aspx (accessed on 13 February 2022).
50. Atangana, A. *Fract. Operators with Constant and Variable Order with Application to Geo-Hydrology*; Academic Press: Cambridge, MA, USA, 2017.
51. Tonina, D.; Buffington, J.M. Hyporheic exchange in gravel bed rivers with pool-riffle morphology: Laboratory experiments and three-dimensional modeling. *Water Resour. Res.* **2007**, *43*, W01421. [CrossRef]
52. Zlatanović, S.; Fabian, J.; Premke, K.; Mutz, M. Shading and sediment structure effects on stream metabolism resistance and resilience to infrequent droughts. *Sci. Total Environ.* **2018**, *621*, 1233–1239. [CrossRef]
53. Jurjovec, J.; Blowes, D.; Ptacek, C.; Mayer, K. Multicomponent reactive transport modeling of acid neutralization reactions in mine tailings. *Water Resour. Res.* **2004**, *40*. [CrossRef]
54. Su, D.; Mayer, K.U.; MacQuarrie, K.T.B. MIN3P-HPC: A High-Performance Unstructured Grid Code for Subsurface Flow and Reactive Transport Simulation. *Math. Geosci.* **2021**, *53*, 517–550. [CrossRef]
55. Su, D.; Mayer, K.U.; MacQuarrie, K.T.B. Numerical investigation of flow instabilities using fully unstructured discretization for variably saturated flow problems. *Adv. Water Res.* **2020**, *143*, 103673. [CrossRef]
56. Arcement, G.J.; Schneider, V.R. Guide for Selecting Manning's Roughness Coefficients for Natural Channels and Floodplains. *U.S. Geol. Surv.* 1989. Available online: https://pubs.er.usgs.gov/publication/wsp2339 (accessed on 13 February 2022).
57. Koiter, A.J.; Owens, P.N.; Petticrew, E.L.; Lobb, D.A. The role of gravel channel beds on the particle size and organic matter selectivity of transported fine-grained sediment: Implications for sediment fingerprinting and biogeochemical flux research. *J. Soils Sediments* **2015**, *15*, 2174–2188. [CrossRef]
58. Aldridge, B.N.; Garrett, J.M. Roughness Coefficients for Stream Channels in Arizona. *U.S. Geol. Surv.* 1973. Available online: https://pubs.usgs.gov/of/1973/0003/report.pdf (accessed on 13 February 2022).
59. Trauth, N.; Schmidt, C.; Maier, U.; Vieweg, M.; Fleckenstein, J.H. Coupled 3-D stream flow and hyporheic flow model under varying stream and ambient groundwater flow conditions in a pool-riffle system. *Water Resour. Res.* **2013**, *49*, 5834–5850. [CrossRef]
60. Maher, K.; Mayer, K.U. The Art of Reactive Transport Model Building. *Elements* **2019**, *15*, 117–118. [CrossRef]
61. Murphy, B.L.; Morrison, R.D. Introduction to Environmental Forensics. 2014. Available online: https://www.elsevier.com/books/introduction-to-environmental-forensics/murphy/978-0-12-404696-2 (accessed on 13 February 2022).